Intermolecular Alkane C-H Bond Activation with $(OC)_3Mn^-$ and $(OC)_2Fe^-$ Negative Ions in the Gas Phase

Richard N. McDonald,* Michael T. Jones, and A. Kasem Chowdhury

Contribution from the Department of Chemistry, Kansas State University, Manhattan, Kansas 66506. *Received February 5, 1990*

Abstract: Only $(OC)_2Fe^-$ reacted with CH_4 and $(CH_3)_4C$ to yield the respective hydridoalkyl adduct negative ions, specifically characterized with the neopentyl adduct. Both $(OC)_3Mn^-$ and $(OC)_2Fe^-$ reacted with the alkanes containing β-CH bonds to form $(adduct - H_2)^-$ product ions. The products from the reactions with C_2H_6 were shown to be the $(OC)_nM(\pi\text{-}C_2H_4)^-$ complexes by the further ion/molecule reactions of the Mn complex: adduct formation with SiH_4 and $(CH_3)_3SiH$, C_2H_4 ligand substitution with SO_2, and up to four H/D exchanges with D_2. The H/D exchanges with D_2 established the reversibility of the β-hydride shifts occurring in intermediate metal complex negative ions. From the reaction efficiency (RE) for the C_2H_6 reaction, RE/(1° C-H bond) was derived. The remaining $(adduct - H_2)^-$ product ions produced from the higher *n*-alkanes and the cycloalkanes were characterized as $(OC)_nM(H)(\eta^3\text{-}C_3H_3R_2)^-$ complexes produced by metal insertion into an allylic C-H bond in the intermediate olefin complexes. Cyclopentane was determined to be typical of secondary C-H bonds in these reactions and RE/(2° C-H bond) was derived. The calculated RE for the reactions of $(OC)_3Mn^-$ with the series propane to *n*-heptane and of $(OC)_2Fe^-$ with propane to *n*-pentane based on the number and types of C-H bonds in the alkane agreed reasonably well with the measured RE. The reactions of $(OC)_3Mn^-$ and $(OC)_2Fe^-$ with $CH_3CD_2CH_3$ gave $(adduct - HD)^-$ and $(adduct - H_2)^-$ product ions and smaller than expected normal isotope effects. The small observed isotope effects were argued to be the result of a normal isotope effect giving the $(adduct - HD)^-$ product and an inverse isotope effect leading to the $(adduct - H_2)^-$ ions. This result showed that the steps in the dehydrogenation mechanism following the initial C-H bond oxidative insertion step contribute to k_{total} and the isotope effects. Analysis of the RE for the reactions with isobutane gave RE/(3° C-H bond) with (RE/(3° C-H bond))/(RE/(1° C-H bond)) ratios of 13 for $(OC)_3Mn^-$ and 6 for $(OC)_2Fe^-$. The small normal isotope effect determined for the reaction of $(OC)_3Mn^-$ with $(CD_3)_3CH$ supported the greater reactivity of the tertiary C-H bond compared to the primary C-H bonds in the initial oxidative insertion step. We conclude that the relative rates for oxidative insertion into C-H bonds by these two transition-metal complex negative ions are tertiary ≥ secondary > primary.

The process of inserting transition-metal centers of atomic and molecular species into C-H bonds of alkanes, alkenes, and arenes,[1] commonly referred to as C-H bond activation, is of general interest in chemistry, surface science, and catalysis. In the condensed phase, numerous examples of intramolecular C-H bond activation were reported in the 1960s and 1970s.[1] However, the long sought after examples of intermolecular C-H activation did not appear until 1982 with the independent reports of Janowicz and Bergman $((\eta^5\text{-}C_5Me_5)Ir(PMe_3)H_2 + h\nu)$,[2] Hoyano and Graham $((\eta^5\text{-}C_5Me_5)Ir(CO)_2 + h\nu)$,[3] and Jones and Feher $((\eta^5\text{-}C_5Me_5)Rh(PMe_3)H_2 + h\nu)$.[4]

The relative reactivities of alkane C-H bonds were determined on the basis of the NMR spectra obtained following photolysis of $(\eta^5\text{-}C_5Me_5)M(PMe_3)H_2$ (M = Ir or Rh) in the neat alkane.[2b,5,6] The intermediates generated from both of these metal complexes appeared to favor oxidative insertion into the primary C-H bonds vs the secondary C-H bonds, and no instance of oxidative insertion into tertiary C-H bonds was observed for either system.[5] However, the authors warned that tertiary C-H insertion products for both the Rh and Ir systems and secondary products in the Rh system might be unstable to the reaction conditions.[5] This latter concern was substantiated in a later study. The initial insertion occurred in all the C-H bonds of the alkane, but the secondary insertion products rearranged rapidly and intramolecularly to the primary products.[6] More recently, Bergman et al.[7] reported oxidative insertion of the intermediate formed by irradiation of $(\eta^5\text{-}C_5Me_5)Ir(PMe_3)H_2$ in liquid xenon into the secondary C-H bonds of adamantane and cyclohexane and the atypical tertiary C-H bond of cubane.

Oxidative insertion into a C-H bond of methane has been reported by photoexcited Fe, Mn, Co, Cu, Zn, Ag, and Au atoms in methane matrices at 15 K; Ca, Ti, Cr, and Ni atoms failed to yield insertion products.[8] An independent study of the photosensitized Cu/CH_4 reaction was reported.[9] It was noteworthy that Al atoms oxidatively inserted into methane *without photolysis*.[10] These results followed previous reports that Zr atoms oxidatively inserted into C-H and C-C bonds of isobutane and neopentane[11] and that the small cluster Fe_2 activated methane while Fe atoms did not.[12]

Oxidative insertion of atomic metal positive ions into C-H and C-C bonds of alkanes larger than methane is well-established in

(1) For reviews on this topic, see: (a) Halpern, J. *Inorg. Chim. Acta* **1985**, *57*, 1897. (b) Crabtree, R. H. *Chem. Rev.* **1985**, *85*, 245. (c) Green, M. L. H.; O'Hare, D. *Pure Appl. Chem.* **1985**, *57*, 1897. (d) Rothwell, I. P. *Polyhedron* **1985**, *4*, 177. (e) Shilov, A. E. *The Activation of Saturated Hydrocarbons by Transition Metal Complexes*; Reidel: Dordrecht, 1984. (f) Parshall, G. W. *Chem. Tech.* **1984**, *14*, 628. (g) Muetterties, E. L. *Chem. Soc. Rev.* **1983**, *12*, 283. (h) Brookhart, M.; Green, M. L. H. *J. Organomet. Chem.* **1983**, *250*, 395. (i) Somorjai, G. *Chemistry in Two Dimensions*; Cornell University Press: Ithaca, NY, 1981. (j) Parshall, G. W. *Homogeneous Catalysis*; Wiley: New York, 1980. (k) James, B. R. *Homogeneous Hydrogenation*; Wiley: New York, 1980; Chapter 7. (l) Muetterties, E. L.; Rhodin, T. N.; Band, E.; Brucker, C. F.; Pretzer, W. R. *Chem. Rev.* **1979**, *79*, 91. (m) Webster, D. E. *Adv. Organomet. Chem.* **1977**, *15*, 147. Parshall, G. W. In *Catalysis*; *Specialist Periodical Report*; The Chemical Society: London, 1977; Vol. 1, 335. (o) Parshall, G. W. *Acc. Chem. Res.* **1975**, *8*, 113. (p) Parshall, G. W. *Homogeneous Hydrogenation*; Wiley: New York, 1973. (q) Parshall, G. W. *Catalysis* **1972**, *1*, 335. (r) Parshall, G. W. *Acc. Chem. Res.* **1970**, *3*, 139. (s) Halpern, J. *Acc. Chem. Res.* **1970**, *3*, 386. (t) Collman, J. P. *Acc. Chem. Res.* **1968**, *1*, 136.

(2) (a) Janowicz, A. H.; Bergman, R. G. *J. Am. Chem. Soc.* **1982**, *104*, 352. (b) Janowicz, A. H.; Bergman, R. G. *J. Am. Chem. Soc.* **1983**, *105*, 3929.

(3) Hoyano, J. K.; Graham, W. A. G. *J. Am. Chem. Soc.* **1982**, *104*, 3723.

(4) (a) Jones, W. D.; Feher, F. J. *J. Am. Chem. Soc.* **1982**, *104*, 4240. (b) Jones, W. D.; Feher, F. J. *J. Am. Chem. Soc.* **1984**, *106*, 1650.

(5) Janowicz, A. H.; Periana, R. A.; Buchanan, J. M.; Kovac, C. A.; Stryker, J. M.; Wax, M. J.; Bergman, R. G. *Pure Appl. Chem.* **1984**, *56*, 13.

(6) Periana, R. A.; Bergman, R. G. *J. Am. Chem. Soc.* **1986**, *108*, 7332.

(7) Sponsler, M. B.; Weiller, B. H.; Stoutland, P. O.; Bergman, R. G. *J. Am. Chem. Soc.* **1989**, *111*, 6841.

(8) Billups, W. E.; Konarski, M. M.; Hauge, R. H.; Margrave, J. L. *J. Am. Chem. Soc.* **1980**, *102*, 7393.

(9) Ozin, G. A.; McIntosh, D. F.; Mitchell, S. A.; Garcia-Prieto, J. *J. Am. Chem. Soc.* **1981**, *103*, 1574.

(10) Klabunde, K. J.; Tanaka, Y. *J. Am. Chem. Soc.* **1983**, *105*, 3544.

(11) Remick, R. J.; Asunta, T. A.; Skell, P. S. *J. Am. Chem. Soc.* **1979**, *101*, 1322.

(12) Barrett, P. H.; Pasternak, M.; Pearson, R. G. *J. Am. Chem. Soc.* **1979**, *101*, 222.

0002-7863/91/1513-476$02.50/0

the gas phase.[13-17] The products of these ion/molecule reactions are those formed by fragmentation of intermediates with loss of a neutral molecule, e.g., H_2, CH_4, C_2H_4, and others. However, methane was generally found to be inert in these studies. The results of several studies using ion beam techniques established that the product-forming channels of the reactions of M^+ with methane yielding $M—CH_3^+$ or $M{=}CH_2^+$ were endothermic.[14,16a,c] The variety of the atomic metal cations employed in these investigations and the metal–ligand bond energies that have been determined are a testimony to the efforts by these investigators and the apparatus and methods used.

By analogy to the condensed-phase results, it appeared that the availability of a single coordination site in a metal complex negative ion would allow for observation of C–H bond activation. This assumption proved to be wrong for the first row 15- ($(OC)_4Cr^-$ and $(OC)_3Fe^-$) and 16-electron ($(OC)_4Mn^-$ and $(OC)_3Co^-$) transition-metal carbonyl negative ions[18] since no reactions of these ions with CH_4 or higher alkanes were observed within the time constraints of our flowing afterflow (FA) experiments ($k < 10^{-13}$ cm^3 molecule^{-1} s^{-1}). However, the development of conditions in the FA to produce the 13-electron $(OC)_2Fe^-$ and 14-electron $(OC)_3Mn^-$ complex ions[19] allowed for studies of C–H bond activation with CH_4 and higher alkanes.[20-22] One point of particular importance from these latter studies is the C–H bond reactivity order, tertiary > secondary > primary observed with $(OC)_3Mn^-$.[20] The details of the generation of these two multicoordinatively and multielectronically unsaturated (MCMEU) transition-metal complex negative ions, $(OC)_3Mn^-$ and $(OC)_2Fe^-$, and the studies of their ion/molecule reactions with methane, several acyclic alkanes, cyclopentane, and cyclohexane are the subject of this paper.

Experimental Section

The FA apparatus used in these investigations has been previously described.[23] Briefly, we first establish and maintain a fast flow of helium in the flow tube. For the present experiments, the flow conditions were P_{He} = 0.8–0.9 Torr and $\bar{v} \approx 55$ m s^{-1}. The electron gun (rhenium filament) is turned on, and the transition-metal carbonyl negative ions of interest are prepared by dissociative electron attachment to small concentrations of $Mn_2(CO)_{10}$ or $Fe(CO)_5$ (latter resevoir cooled in ice–water) continuously added at inlet 1. The initially formed excited metal carbonyl negative ions are cooled to their vibrational ground states by numerous collisions with the helium buffer gas in the first 75 cm of the ~1.5-m-long flow tube. Neutral reactants are introduced to the ion/He flow via a gas inlet, and the ion/molecule reaction occurs in the final 65 cm of the flow tube. The flow is sampled through 1-mm orifices in two nose cones into a differentially pumped compartment ($P \approx 10^{-7}$ Torr) containing the quadrupole mass filter and electron multiplier that continuously monitor the ion composition of the flow. Neutral reaction products are not directly observed but are assumed on the basis of mass balance and thermochemistry.

The kinetics of these bimolecular ion/molecule reactions are determined under pseudo-first-order conditions where the concentration of the added neutral molecules ([N]) is in large excess compared to the ion concentration. In our experiments, we maintain the reaction distance (time) constant and vary the concentration of the added neutral. From a series of such measurements, the slope of the linear decay of the starting ion signal from a plot of log [ion signal] vs increasing [N] added to the flow is converted to the bimolecular rate constant by equations already given.[23b] The FAs kinetic window of 10^4 allows us to measure rate constants for reactions that occur on every collision ($k \approx 10^{-9}$ cm^3 molecule^{-1} s^{-1}) and those that occur in one out of every 10 000 collisions ($k = 10^{-13}$ cm^3 molecule^{-1} s^{-1}).

Metal Complex Negative Ion Generation. The method developed to generate the mixtures of metal complex negative ions $(OC)_{4,3,2}Fe^-$ and $(OC)_{5,4,3}Mn^-$ was based on mass spectrometry appearance potential (AP) data for several transition-metal carbonyl molecules.[24] The monometal carbonyls $M(CO)_x$ (M = Cr, W, Fe, and Ni) undergo dissociative electron attachment with thermal or near-thermal energy electrons to yield the $(OC)_{x-1}M^-$ negative ions. The AP data suggested that if the energy of the impacting electron was increased by up to several electronvolts, the $(OC)_{x-2}M^-$ and $(OC)_{x-3}M^-$ negative ions would be produced; such ions had been previously observed in ion cyclotron resonance spectrometers.[25]

In the FA, the relatively high pressure of the helium buffer gas moderates the electron energy, thus allowing for generation of thermal or near-thermal energy electrons. Our initial experiments were carried out with the electron gun placed in the center of the flow tube, and a small flow of $Fe(CO)_5$ was passed over the electron gun. When the emission current of the electron gun was substantially increased,[26] a broad distribution of electron energies was produced and we observed formation of the $(OC)_{3,4}Fe^-$ mixture. However, the downstream flow contained considerable free electrons and photons from the hot plasma formed at the electron gun. Therefore, ion production occurred throughout the length of the flow tube.

The ion generation region was redesigned, and a helium inlet, the electron gun, and the volatile metal carbonyl inlet were placed in a Pyrex side arm attached to the main flow tube at a 90° angle.[23a] About 10% of the helium buffer gas is added via the inlet at the bottom of the side arm to allow for the electron/ion plasma formation with the remaining helium introduced at the upstream end of the main flow tube. The reduced helium concentration in the side arm (a pressure differential between the side arm and the main flow tube is assumed) should yield a broad distribution of electron energies for dissociative attachment to the neutral metal carbonyl molecules. The observed product is a mixture of metal carbonyl negative ions containing varying numbers of CO ligands. By use of this design, the photons and most of the excess free electrons are removed from the upstream flow since they did not make the 90° turn into the main flow tube.[27]

One problem is that the minimum electron energy needed to effect loss of three CO ligands from $Fe(CO)_5$ to form $(OC)_2Fe^-$ greatly exceeds the EA$(Fe(CO)_3)$ = 1.8 ± 0.2 eV and EA$(Fe(CO)_2)$ = 1.22 ± 0.02 eV[28]

(13) (a) Allison, J.; Freas, R. B.; Ridge, D. P. *J. Am. Chem. Soc.* **1979**, *101*, 1332. (b) Larsen, B. S.; Ridge, D. P. *J. Am. Chem. Soc.* **1984**, *106*, 1912.

(14) For a recent review of this subject, see: Armentrout, P. B. In *Gas Phase Inorganic Chemistry*; Russell, D. H., Ed.; Plenum Press: New York, 1989; Chapter 1.

(15) (a) Byrd, G. D.; Burnier, R. C.; Freiser, B. S. *J. Am. Chem. Soc.* **1982**, *104*, 3565. (b) Byrd, G. D.; Freiser, B. S. *J. Am. Chem. Soc.* **1982**, *104*, 5944. (c) Jacobson, D. B.; Freiser, B. S. *J. Am. Chem. Soc.* **1983**, *105*, 736, 5197, 7484, 7492. (d) Jacobson, D. B.; Byrd, G. D.; Freiser, B. S. *Inorg. Chem.* **1984**, *23*, 553. (e) Jackson, T. C.; Carlin, T. J.; Freiser, B. S. *J. Am. Chem. Soc.* **1986**, *108*, 1120.

(16) (a) Armentrout, P. B.; Beauchamp, J. L. *J. Am. Chem. Soc.* **1981**, *103*, 784. (b) Armentrout, P. B.; Halle, L. F.; Beauchamp, J. L. *J. Am. Chem. Soc.* **1981**, *103*, 6501, 6624, 6628. (c) Halle, L. F.; Armentrout, P. B.; Beauchamp, J. L. *Organometallics* **1982**, *1*, 963. (d) Halle, L. F.; Houriet, R.; Kappes, M. M.; Staley, R. H.; Beauchamp, J. L. *J. Am. Chem. Soc.* **1982**, *104*, 6293. (e) Tolbert, M. A.; Beauchamp, J. L. *J. Am. Chem. Soc.* **1984**, *106*, 8117.

(17) Radecki, B. D.; Allison, J. *Organometallics* **1986**, *5*, 411.

(18) McDonald, R. N.; Chowdhury, A. K.; Schell, P. L. *J. Am. Chem. Soc.* **1984**, *106*, 6095. McDonald described the generation and some reactions of $(OC)_3Fe^-$. Similar conditions will produce the other 15- and 16-electron, first-row transition-metal complex negative ions starting with the mono- or dinuclear metal carbonyls.

(19) McDonald, R. N.; Chowdhury, A. K.; Jones, M. T. *J. Am. Chem. Soc.* **1986**, *108*, 3105.

(20) McDonald, R. N.; Jones, M. T. *J. Am. Chem. Soc.* **1986**, *108*, 8097.

(21) McDonald, R. N.; Jones, M. T. *Organometallics* **1987**, *6*, 1991.

(22) McDonald, R. N.; Reed, D. J.; Chowdhury, A. K. *Organometallics* **1989**, *8*, 1122.

(23) (a) McDonald, R. N.; Chowdhury, A. K. *J. Am. Chem. Soc.* **1985**, *107*, 4123. (b) McDonald, R. N.; Chowdhury, A. K.; Setser, D. W. *J. Am. Chem. Soc.* **1980**, *102*, 6491.

(24) Pignatoro, S.; Foffani, A.; Grasso, F.; Cantone, B. *Z. Phys. Chem. (Munich)* **1965**, *47*, 106. (b) Winters, R. E.; Kiser, R. W. *J. Chem. Phys.* **1966**, *44*, 1964. (c) Sullivan, R. E.; Kiser, R. W. *J. Chem. Phys.* **1968**, *49*, 1978. (d) Compton, R. N.; Stockdale, J. A. D. *Int. J. Mass Spectrom. Ion Phys.* **1976**, *22*, 47.

(25) (a) Dunbar, R. C.; Ennever, J. F.; Fackler, J. P. *Inorg. Chem.* **1973**, *12*, 2734. (b) Foster, M. S.; Beauchamp, J. L. *J. Am. Chem. Soc.* **1975**, *97*, 4808. (c) Richardson, J. H.; Stephenson, L. M.; Brauman, J. I. *J. Am. Chem. Soc.* **1974**, *96*, 3671. (d) Rynard, C. M.; Brauman, J. I. *Inorg. Chem.* **1980**, *19*, 3544. (e) Wronka, J.; Ridge, D. P. *J. Am. Chem. Soc.* **1984**, *106*, 67.

(26) The electron gun's emission current is a measure of the electron/ion plasma density between the filament held at −100 to −400 V negative potential and a grounded tungsten mesh grid located 1 cm downstream of the filament. For thermal energy electron production, the emission current is <80 μA with use of a thorium oxide coated iridium filament. To increase the emission current, the amperage and negative potential supplied to the rhenium filament are increased.

(27) A minor shortcoming of this new design is that ions generated in the side arm with masses <~30 amu (e.g., $F^- \leftarrow NF_3 + e^-$) also do not appear to make this 90° turn since they are not observed by the quadrupole mass filter and electron multiplier. However, these low-mass ions may still be used to effect reactions by inletting other neutrals at the upstream end of the flow tube (e.g., $F^- + C_6H_5C(=O)CH_3 \rightarrow C_6H_5C(O^-){=}CH_2 + HF$), generating large ion signals for the product ions.

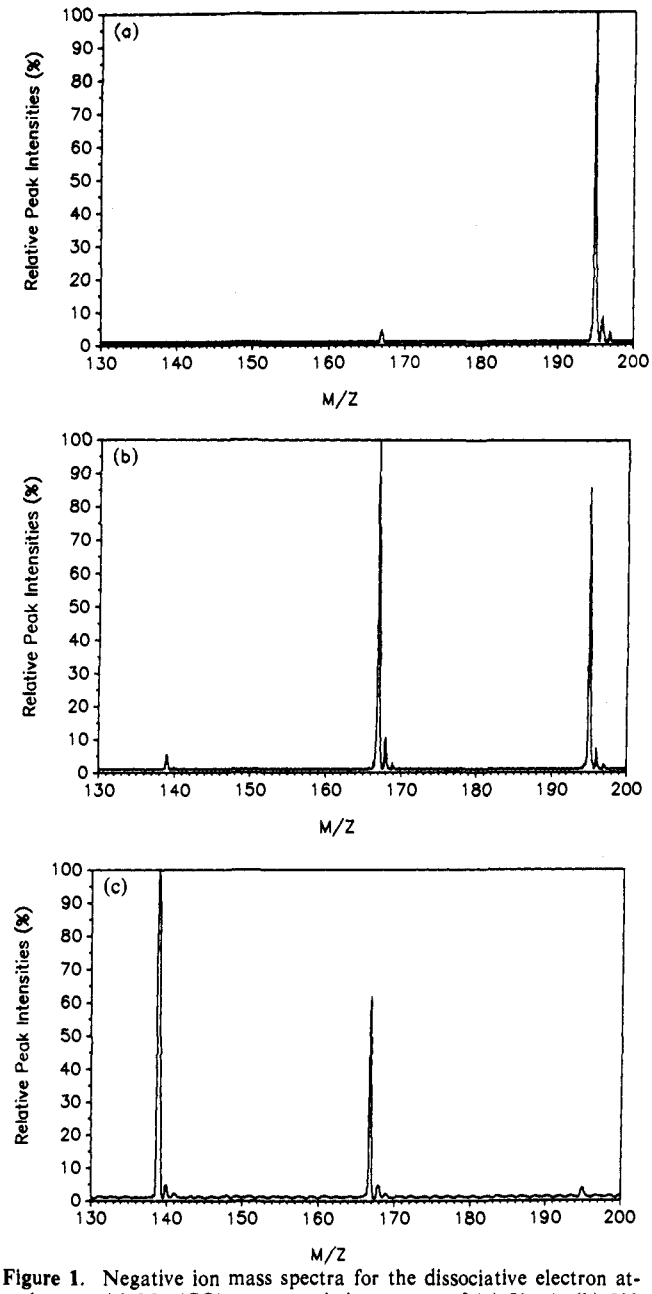

Figure 1. Negative ion mass spectra for the dissociative electron attachment with $Mn_2(CO)_{10}$ at an emission current of (a) 50 μA, (b) 500 μA, and (c) 4 mA.

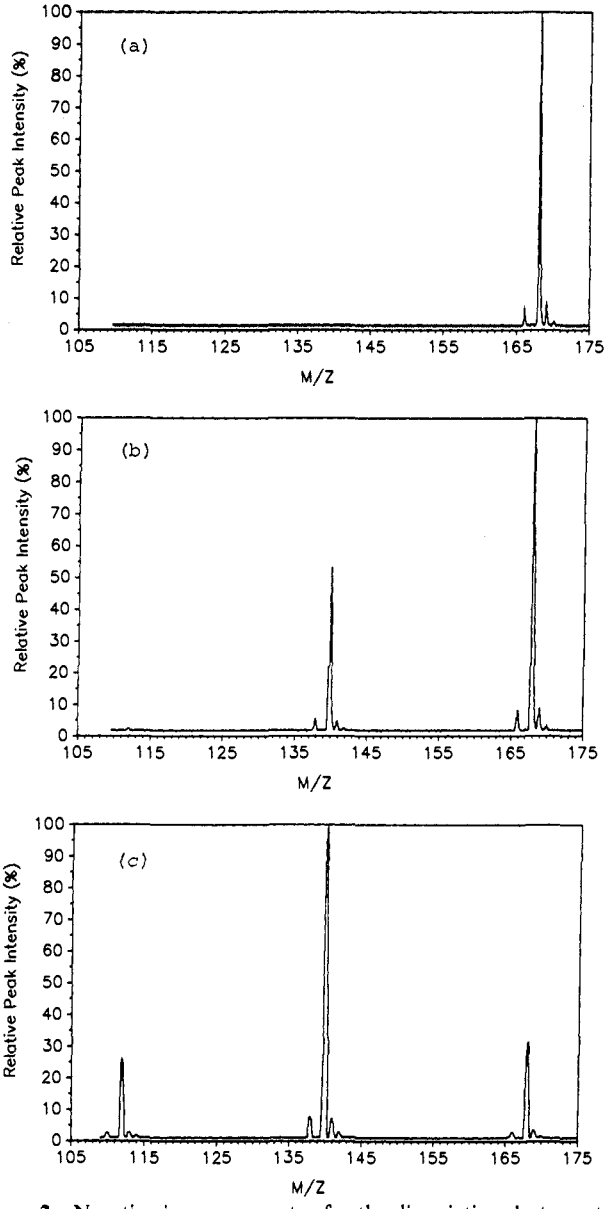

Figure 2. Negative ion mass spectra for the dissociative electron attachment with $Fe(CO)_5$ at an emission current of (a) 500 μA, (b) 1.5 mA, and (c) 8 mA.

(EA, electron affinity), and electron autodetachment could occur. It appears that much of the excess energy is removed as internal and translational energy by the three dissociated CO molecules with the residual energy present in the MCMEU metal complex negative ions less than the EA of the neutral metal carbonyl complex. The use of the higher total P_{He} was to yield a better distribution of electron energies for dissociative attachment to the neutral metal carbonyl and to improve the collisional cooling of the excited MCMEU metal carbonyl negative ions formed. For whatever reason, the total P_{He} = 0.8–0.9 Torr is optimum for generating $(OC)_2Fe^-$ and $(OC)_3Mn^-$. At $P_{He} < 0.5$ or $P > 1.1$ Torr, these ion signals are not observed. Attempts to find better operating conditions for generating these MCMEU metal complex negative ions by varying P_{He}, changing the distribution of helium between the side arm and the main flow tube, and changing the electron gun's emission current have failed. Thus, our ability to vary the flow tube pressure with sufficient signal intensity for these ions is greatly restricted compared to conventional FA experiments.

Under these conditions, we are able to control the ion composition present in the flow using this design by careful control of the amount of the metal carbonyl added and the emission current of the electron gun.[26] This is shown in Figures 1 and 2 for the ion series $(OC)_{3,4,5}Mn^-$ and $(OC)_{2,3,4}Fe^-$, respectively. Not shown in Figures 1 and 2 are the dinuclear metal carbonyl negative ions (relative intensities given) also formed under these conditions: $Mn_2(CO)_9^-$, large at 50 μA; $Mn_2(CO)_{7-9}^-$, small at 500 μA and a trace at 5 mA; and $Fe_2(CO)_{7,8}^-$, small at <500 μA, smaller at 1.5 mA, and a trace at 8 mA. None of these dinuclear cluster negative ions reacted with the hydrocarbons used in this study. With these three sets of operating conditions, the separate ion/molecule chemistry (rate constants and products) of each mononuclear metal carbonyl negative ion can be determined. An obvious constraint in dealing with mixtures of ions is that the mass of the reaction products of one ion do not coincide with the masses of other starting ions or their product ions. Even if this should happen, there are usually methods available to sort out the problem. Some examples of these methods will be mentioned in this paper.

The higher emission current needed to generate $(OC)_2Fe^-$ compared to $(OC)_3Mn^-$ produced considerably more free, low-energy electrons in the downstream flow for the former negative ion studies. These electrons were capable of producing $(OC)_4Fe^-$ from excess $Fe(CO)_5$ but not $(OC)_{2,3}Fe^-$. This, coupled with the small intensity of the $(OC)_2Fe^-$ ion signal, the larger relative amount of $(OC)_3Fe^-$ present, and the greater reactivity of $(OC)_{3,4}Fe^-$ vs $(OC)_{4,5}Mn^-$ with added neutrals usually made it difficult (or impossible) to obtain unambiguous results of the structures of the primary reaction product ions derived from $(OC)_2Fe^-$ from their further ion/molecule reactions. The results of such studies were more

(28) Engelking, P. C.; Lineberger, W. C. *J. Am. Chem. Soc.* **1979**, *101*, 5569.

Table I. Summary of Kinetic and Product Data for the Reactions of $(OC)_3Mn^-$ with Acyclic and Cyclic Alkanes

reactn no.	alkane	product ion [+assumed neutral(s)]	branching fraction	k_{total},[a] cm^3 $molecule^{-1}$ s^-	k_{ADO},[b] cm^3 $molecule^{-1}$ s^{-1}	reactn effic[c]
1	CH_4	no reaction		$<10^{-13}$		
2	$(CH_3)_4C$	no reaction		$<10^{-13}$		
3	C_2H_6	$(OC)_3Mn(C_2H_4)^-$ [$+H_2$]	1.00	$(9.2 \pm 0.1) \times 10^{-12}$	1.0×10^{-9}	0.0092
4	C_2D_6	$(OC)_3Mn(C_2D_4)^-$ [$+D_2$]	1.00	$(4.1 \pm 0.1) \times 10^{-12}$	1.0×10^{-9}	
5	c-C_5H_{10}	$(OC)_3Mn(H)(c\text{-}C_5H_7)^-$ [$+H_2$]	1.00	$(1.1 \pm 0.1) \times 10^{-10}$	1.0×10^{-9}	0.11
6	c-C_6H_{12}	$(OC)_3Mn(H)(c\text{-}C_6H_9)^-$ [$+H_2$]	1.00	$(4.4 \pm 0.8) \times 10^{-11}$	1.1×10^{-9}	0.040
7	c-C_6D_{12}	$(OC)_3Mn(D)c\text{-}C_6D_9)^-$ [$+D_2$]	1.00	$(1.3 \pm 0.1) \times 10^{-11}$		0.012
8	C_3H_8	$(OC)_3Mn(H)(C_3H_5)^-$ [$+H_2$]	1.00	$(2.5 \pm 0.2) \times 10^{-11}$	1.0×10^{-9}	0.025
9a	$CH_3CD_2CH_3$	$(OC)_3Mn(H)(C_3H_4D)^-$ [+HD]	0.47	$(2.1 \pm 0.2) \times 10^{-11}$		0.021
9b		$(OC)_3Mn(D)(C_3H_4D)^-$ [$+H_2$]	0.53			
10	$CH_3(CH_2)_2CH_3$	$(OC)_3Mn(H)(C_4H_7)^-$ [$+H_2$]	1.00	$(4.6 \pm 0.1) \times 10^{-11}$	1.0×10^{-9}	0.046
11	$CH_3(CH_2)_3CH_3$	$(OC)_3Mn(H)(C_5H_9)^-$ [$+H_2$]	1.00	$(1.1 \pm 0.1) \times 10^{-10}$	1.1×10^{-9}	0.10
12	$CH_3(CH_2)_4CH_3$	$(OC)_3Mn(H)(C_6H_{11})^-$ [$+H_2$]	1.00	$(1.2 \pm 0.1) \times 10^{-10}$	1.1×10^{-9}	0.11
13	$CH_3(CH_2)_5CH_3$	$(OC)_3Mn(H)(C_7H_{13})^-$ [$+H_2$]	1.00	$(2.2 \pm 0.2) \times 10^{-10}$	1.1×10^{-9}	0.20
14	$(CH_3)_3CH$	$(OC)_3Mn(H)(C_4H_7)^-$ [$+H_2$]	1.00	$(3.9 \pm 0.2) \times 10^{-11}$	1.2×10^{-9}	0.033
15a	$(CD_3)_3CH$	$(OC)_3Mn(D)(C_4D_7)^-$ [+HD]	0.54	$(3.0 \pm 0.1) \times 10^{-11}$		0.025
15b		$(OC)_3Mn(H)(C_4D_7)^-$ [$+D_2$]	0.46			

[a] These values are averages of at least two separate measurements. The listed errors are the maximum deviations in the measured rate constants from this average value, which is generally $\leq \pm 10\%$. The errors due to systematic uncertainties in calibrations suggest that their accuracy is $\pm 20\%$ for external comparisons. [b] The collision-limited rate constants were calculated by the average dipole orientation theory, k_{ADO}. [c] Defined as k_{total}/k_{ADO}.

Table II. Summary of Kinetic and Product Data for the Reactions of $(OC)_2Fe^-$ with Acyclic and Cyclic Alkanes

reactn no.	alkane	product ion [+assumed neutral(s)]	branching fraction	k_{total},[a] cm^3 $molecule^{-1}$ s^{-1}	k_{ADO},[b] cm^3 $molecule^{-1}$ s^{-1}	reactn effic[c]
1	CH_4	$(OC)_2Fe(H)(CH_3)^-$	1.00	$(2.6 \pm 0.5) \times 10^{-13}$ [d]		
2	$(CH_3)_4C$	$(OC)_2Fe(H)(CH_2C(CH_3)_3)^-$	1.00	$(7.1 \pm 0.5) \times 10^{-12}$ [d]		
3	C_2H_6	$(OC)_2Fe(C_2H_4)^-$ [$+H_2$]	1.00	$(1.5 \pm 0.1) \times 10^{-11}$	1.0×10^{-9}	0.015
4	C_2D_6	$(OC)_2Fe(C_2D_4)^-$ [$+D_2$]	1.00	$(5.6 \pm 0.8) \times 10^{-12}$		0.0056
5	c-C_5H_{10}	$(OC)_2Fe(C_5H_8)^-$ [$+H_2$]	1.00	$(2.1 \pm 0.1) \times 10^{-10}$	1.0×10^{-9}	0.21
6	c-C_6H_{12}	$(OC)_2Fe(C_6H_{10})^-$ [$+H_2$]	1.00	$(2.8 \pm 0.3) \times 10^{-11}$	1.1×10^{-9}	0.025
7	c-C_6D_{12}	$(OC)_2Fe(C_6D_{10})^-$ [$+D_2$]	1.00	$(5.6 \pm 0.3) \times 10^{-12}$		0.0051
8	C_3H_8	$(OC)_2Fe(C_3H_6)^-$ [$+H_2$]	1.00	$(3.9 \pm 0.1) \times 10^{-11}$	1.0×10^{-9}	0.039
9a	$CH_3CD_2CH_3$	$(OC)_2Fe(C_3H_5D)^-$ [+HD]	0.73	$(3.9 \pm 0.1) \times 10^{-11}$		0.039
9b		$(OC)_2Fe(C_3H_4D_2)^-$ [$+H_2$]	0.27			
10	$CH_3(CH_2)_2CH_3$	$(OC)_2Fe(C_4H_8)^-$ [$+H_2$]	1.00	$(1.3 \pm 0.1) \times 10^{-10}$	1.0×10^{-9}	0.13
11	$CH_3(CH_2)_3CH_3$	$(OC)_2Fe(C_5H_{10})^-$ [$+H_2$]	1.00	$(1.8 \pm 0.1) \times 10^{-10}$	1.1×10^{-9}	0.16
12	$(CH_3)_3CH$	$(OC)_2Fe(C_4H_8)^-$ [$+H_2$]	1.00	$(4.4 \pm 0.2) \times 10^{-11}$	1.2×10^{-9}	0.037

[a–c] See Table I. [d] The apparent bimolecular rate constant (k_{app}) for what is assumed to be a termolecular reaction yielding the adduct negative ion.

readily observed and interpreted for the primary product ions formed in the ion/molecule reactions of $(OC)_3Mn^-$ and the alkanes. We assume that these results apply to the structures of the product ions from both MCMEU metal complex negative ions.

The mechanism for forming the lower molecular weight MCMEU negative ions is assumed to involve stepwise loss of CO ligands from the excited parent complex negative ions $[Mn(CO)_5^-]^*$ and $[Fe(CO)_5^-]^*$. This would be similar to the mechanism proposed for the single-photon photofragmentation of $Fe(CO)_5$.[29]

Results

The kinetic and product data for the reactions of $(OC)_3Mn^-$ and $(OC)_2Fe^-$ with the acyclic and cyclic alkanes are listed in Tables I and II, respectively. The primary chemistry of the two MCMEU ions reacting with the alkanes and cycloalkanes is easy to determine since the ions $(OC)_{4,5}Mn^-$ and $(OC)_{3,4}Fe^-$ did not react with these hydrocarbons. However, as pointed out above, structural characterization of the primary ion products largely rests on the results of the further ion/molecule reactions of the ion products formed in the $(OC)_3Mn^-$ reactions.

In all of the experiments, linear pseudo-first-order decay plots of the log [ion signal] vs increasing concentration of the added neutral substrate were observed. The primary product branching fractions given in Tables I and II were the relative product ion signals obtained by integration of the negative ion spectra (averages of 10–15 spectra to increase signal to noise ratios) taken at 6–8 different concentrations of added neutral substrate during the kinetic run. These branching fractions did not vary outside of our experimental error (±3% absolute) through >95% decay of the starting ion signal. Unless otherwise noted, >90% of the decay of the integrated starting ion signal was observed as product ion(s) signal intensity.

Discussion

Reactions with Methane and Neopentane. Only $(OC)_2Fe^-$ reacted with CH_4 to produce the adduct at m/z 128 (eq 1; Table II).[30] However, the reaction proceeded at the lower limit of the

$$\underset{m/z\ 112}{(OC)_2Fe^-} + CH_4 \xrightarrow{He} \underset{m/z\ 128}{(OC)_2Fe(CH_4)^-} \qquad (1)$$

FA experiment with a very small amount of adduct product ions at m/z 128 formed and the concomitant small attenuation in the

(29) Yardley, J. T.; Gitlin, B.; Nathanson, G.; Rosan, A. M. *J. Chem. Phys.* **1981**, *74*, 370.

(30) A reviewer suggested that the ion product at m/z 128 could be $(OC)_2FeO^-$ formed by reaction of $(OC)_{2-4}Fe^-$ with O_2 contamination in the CH_4 sample or in the inlet lines. For the reaction of $(OC)_4Fe^-$ with O_2, see: Lane, K.; Sallans, L.; Squires, R. R. *J. Am. Chem. Soc.* **1984**, *106*, 2719. Reexamination of the reaction of $(OC)_{2-4}Fe^-$ with CH_4 produced the same results given in the text. The $Fe(CO)_5$ reservoir was replaced with one containing $Mn_2(CO)_{10}$, and a mixture of $(OC)_{3-5}Mn^-$ ions was generated. *No reaction was observed when up to* $\sim 5 \times 10^{14}$ *molecules* cm^{-3} *of the sample of* CH_4 *used above was added*; using larger concentrations of CH_4 produced a small ion signal at m/z 155, presumably due to the $(OC)_3Mn(H)(CH_3)^-$ ion or an ion/neutral cluster. We had previously found that the reaction of $(OC)_4Mn^-$ with O_2 ($k_{total} = 4.9 \times 10^{-11}$ cm^3 $molecule^{-1}$ s^{-1}) was twice as efficient as the reaction of $(OC)_4Fe^-$ with O_2 and produced the four primary ions (branching fractions) $(OC)_2MnO_2^-$ (0.55; m/z 143), $(OC)_3MnO_2^-$ (0.18; m/z 171), $(OC)_3MnO^-$ (0.18; m/z 155), and $(OC)_2MnO^-$ (0.09; m/z 127) terminating in the ions MnO_3^- (m/z 103) and MnO_4^- (m/z 119). See: Jones, M. T. Ph.D. Thesis, Kansas State University, 1987. These results are consistent with our interpretation given in the text and show that the rate constant for the reaction of $(OC)_3Mn^-$ with CH_4 is at least 50 times less than that measured for the analogous reaction with $(OC)_2Fe^-$.

starting ion signal at m/z 112. Since our structural characterization of ion products depends on their further ion/molecule chemistry, the structure of the ions at m/z 128 could not be probed directly.

Formation of adduct products from ion/molecule reactions is considered to require collisional stabilization of the adduct ion with the helium buffer gas to be observed; these are formally termolecular processes. We then examined the reaction of $(OC)_2Fe^-$ with $(CH_3)_4C$, which should significantly increase the density of states of the corresponding adduct product ions and its lifetime, thereby increasing the efficiency of collisional stabilization of the adduct. This approach proved correct with formation of the adduct ions at m/z 184 (eq 2), and the apparent

$$\underset{m/z\ 112}{(OC)_2Fe^-} + (CH_3)_4C \xrightarrow{He} \underset{m/z\ 184}{(OC)_2Fe(H)(CH_2C(CH_3)_3)^-} \quad (2)$$

bimolecular rate constant increased by a factor of 30 compared to that for reaction 1 (Table II). $(OC)_3Mn^-$ also failed to react with $(CH_3)_4C$ ($k < 10^{-13}$ cm^3 molecule^{-1} s^{-1}).

To identify the structure of the adduct ions in eq 2 at m/z 184, H_2 was added to the flow downstream of the $(CH_3)_4C$ gas inlet. While no reaction was observed between H_2 and the adduct ions at m/z 184, the unreacted $(OC)_2Fe^-$ ions present in the flow readily formed $(OC)_2Fe(H)_2^-$ (m/z 114) and $(OC)_2Fe(H)_4^-$ (m/z 116).[19] In separate experiments, it was shown that neither of the hydrides at m/z 114 and 116 reacted with $(CH_3)_4C$. When D_2 was added to the flow containing the adduct ions at m/z 184, the product ions of a *single H/D exchange* at m/z 185 resulted (eq 3). The product ions formed by adding D_2 to unreacted $(OC)_2Fe^-$,

$$\underset{m/z\ 184}{(OC)_2Fe(H)(CH_2C(CH_3)_3)^-} + D_2 \rightarrow \underset{m/z\ 185}{(OC)_2Fe(D)(CH_2C(CH_3)_3)^-} + HD \quad (3)$$

$(OC)_2Fe(D)_2^-$, and $(OC)_2Fe(D)_4^-$[19] were separately shown not to react with $(CH_3)_4C$. Further, the adduct ions at m/z 184 reacted with H_2S to yield product (adduct $- H_2)^-$ (m/z 216) and (adduct $- CO-H_2)^-$ (m/z 188) ions (eq 4). Either one or both

$$\underset{m/z\ 184}{(OC)_2Fe(H)(CH_2C(CH_3)_3)^-} + H_2S \rightarrow \underset{m/z\ 216}{(OC)_2Fe(SH)(CH_2C(CH_3)_3)^-} + H_2 \quad (4a)$$

$$\rightarrow \underset{m/z\ 188}{(OC)Fe(SH)(CH_2C(CH_3)_3)^-} + CO + H_2 \quad (4b)$$

of the product ions at m/z 216 and 188 in reaction 4 could logically have the corresponding sulfide–hydride structures since neither reacted further with excess H_2S.

The above results in reactions 3 and 4 are consistent with the structure of the adduct ions at m/z 184 formed in reaction 2 having a unique Fe–H bond as shown in the hydride–alkyl complex negative ion $(OC)_2Fe(H)(CH_2C(CH_3)_3)^-$. These results rule out the 17-electron complexes $(OC)_2Fe(H)_2(=CHC(CH_3)_3)^-$ (formed by α-hydride shift) or $(OC)_2Fe(CH_3)(H)(\pi\text{-}CH_2{=}C(CH_3)_2)^-$ (formed by β-methyl shift) as structures of the adduct at m/z 184 since other 17-electron complexes[31] do not react with H_2 or D_2. By analogy, we argue that the product adduct ions at m/z 128 in reaction 1 are also the metal complex negative ions $(OC)_2Fe(H)(CH_3)^-$.

Reactions with Ethane. The examples above of the reactions of $(OC)_2Fe^-$ with CH_4 and $(CH_3)_4C$ ruled out α-hydrogen or β-methyl migrations to Fe in the C–H bond oxidative insertion adduct ion products since ejection of H_2 or CH_4, respectively, should have occurred, leading to the products of an overall bimolecular process. However, the corresponding reactions with ethane open up the possibility for the well-known β-hydrogen migration to occur following oxidative insertion into a primary C–H bond. Reductive elimination of H_2 from the excited adduct ions would then yield the (adduct $- H_2)^-$ product ions.

(31) McDonald, R. N.; Schell, P. L. *Organometallics* **1988**, *7*, 1806, 1820.

Table III. Summary of the Reactivity of the Product Ions Formed in the Reactions of $(OC)_3Mn^-$ and the Hydrocarbons with SO_2

hydrocarbon reactant	product ion examined	k_{total},[a,b] cm^3 molecule^{-1} s^{-1}
C_2H_6	$(OC)_3Mn(C_2H_4)^-$	$(8.0 \pm 0.6) \times 10^{-10}$
C_3H_8	$(OC)_3Mn(H)(C_3H_5)^-$	$(1.3 \pm 0.2) \times 10^{-11}$
$(CH_3)_3CH$	$(OC)_3Mn(H)(C_4H_7)^-$	$(1.5 \times 10^{-11})^c$
$CH_3(CH_2)_3CH_3$	$(OC)_3Mn(H)(C_5H_9)^-$	$(2.5 \times 10^{-11})^c$
$CH_3(CH_2)_4CH_3$	$(OC)_3Mn(H)(C_6H_{11})^-$	$(2.4 \times 10^{-11})^c$
$CH_3(CH_2)_5CH_3$	$(OC)_3Mn(H)(C_7H_{13})^-$	$(3.8 \times 10^{-11})^c$

[a] See Table I. [b] The single ion product of these reactions was $(OC)_3Mn(SO_2)^-$ at m/z 203. [c] From a single kinetic determination.

This was the case when both MCMEU negative ion metal complexes reacted with ethane where $(OC)_2Fe^-$ reacted almost twice as fast as did $(OC)_3Mn^-$ (eqs 5 and 6; Tables I and II). That

$$\underset{m/z\ 139}{(OC)_3Mn^-} + C_2H_6 \rightarrow \underset{m/z\ 167}{(OC)_3Mn(\pi\text{-}C_2H_4)^-} + H_2 \quad (5)$$

$$\underset{m/z\ 112}{(OC)_2Fe^-} + C_2H_6 \rightarrow \underset{m/z\ 140}{(OC)_2Fe(\pi\text{-}C_2H_4)^-} + H_2 \quad (6)$$

we are able to observe these two reactions means that $D°((OC)_nM^-\text{–}C_2H_4) \geq 32.7$ kcal mol^{-1}, the endothermicity for dehydrogenation of C_2H_6, assuming no energy change in the bonding within the $(OC)_nM$ groups on going from starting to product ions.

The product ions of reactions 5 and 6 have the same masses as the $(OC)_4Mn^-$ and $(OC)_3Fe^-$ ions, respectively, which are also present in the separate flows. Since neither $(OC)_4Mn^-$ nor $(OC)_3Fe^-$ reacts with ethane, the formation of the products from reactions 5 and 6 is followed by increases in the integrated ion signals at these masses. In this manner, we are able to account for >90% of the product ions from reaction 5 and ~80% of the product ions from reaction 6; the difference in these two percentages depends on the relative ion signal intensities of $(OC)_{2,3}Fe^-$ and $(OC)_{3,4}Mn^-$ present in the starting ion mixture (Figures 1 and 2). This problem can be avoided by use of C_2D_6 as the neutral substrate where the product ions are observed at m/z 171 and 144. From the rate constants measured for the reactions of the MCMEU metal complex negative ions with C_2H_6 and C_2D_6, kinetic deuterium isotope effects are derived for $(OC)_3Mn^-$, $k_{C_2H_6}/k_{C_2D_6} = 2.2 \pm 0.2$, and for $(OC)_2Fe^-$, $k_{C_2H_6}/k_{C_2D_6} = 3.2 \pm 0.2$.

Although the (adduct $- H_2)^-$ product ions from reactions 5 and 6 did not show evidence of reaction with H_2, they did react with D_2 to form the products of multiple H/D exchange (Table III). This was most clearly observed in the reaction of $(OC)_3Mn(\pi\text{-}C_2H_4)^-$ (m/z 167) with D_2 shown in eq 7 due to the larger con-

$$\underset{m/z\ 167}{(OC)_3Mn(C_2H_4)^-} + D_2 \rightarrow \underset{m/z\ 168\text{–}171}{(OC)_3Mn(\pi\text{-}C_2H_{4-x}D_x)^-} + xHD \qquad x = 1\text{–}4 \quad (7)$$

centration of these ions present compared to those in reaction 6 and the absence of Mn isotopes in reaction 7. The formation of product ions with up to three H/D exchanges (m/z 168–170) was readily observed depending on how much D_2 was added to the flow. While it is probable that a fourth H/D exchange occurred, we could not rule out the possibility that a small amount of $(OC)_4Mn^-$ present in the ion signal at m/z 167 would form the adduct $(OC)_4Mn(D)_2^-$ (m/z 171) with D_2. This latter reaction was shown separately to have an apparent bimolecular rate constant 10 times smaller than the rate constant measured for reaction 7.

This result suggests that the product ions from reactions 5 and 6 are the 16- and 15-electron π-ethylene complexes, respectively, as shown. This structural assignment is consistent with the additional reactions of $(OC)_3Mn(\pi\text{-}C_2H_4)^-$ (m/z 167) with SiH_4 and $(CH_3)_3SiH$ yielding the corresponding adducts and with SO_2

Scheme I

$$(OC)_nM^- + C_2H_6 \rightleftharpoons [(OC)_nM^-/C_2H_6] \rightleftharpoons$$
$$\mathbf{1}$$
$$[(OC)_nM(H)(C_2H_5)^-] \rightleftharpoons [(OC)_nM(H)_2(\pi\text{-}C_2H_4)^-] \rightleftharpoons$$
$$\mathbf{2} \qquad\qquad \mathbf{3}$$
$$[(OC)_nM(\pi\text{-}C_2H_4)^-/H_2] \longrightarrow (OC)_nM(\pi\text{-}C_2H_4)^- + H_2$$
$$\mathbf{4}$$

forming the product ions at m/z 203 in a *fast ligand substitution reaction*[31] (eq 8; Table III). We note here that the reaction of

$$\underset{m/z\ 167}{(OC)_3Mn(\pi\text{-}C_2H_4)^-} + SO_2 \rightarrow \underset{m/z\ 203}{(OC)_3Mn(SO_2)^-} + C_2H_4 \quad (8)$$

$(OC)_3Mn^-$ with ethylene also produced the adduct ions at m/z 167. These latter adduct product ions underwent the same ion/molecule reactions with the same rate constants as the (adduct $- H_2)^-$ product ions at this mass from reaction 5, where they were separately measured.

The general mechanism for the reactions of the MCMEU metal complex negative ions with ethane is shown in Scheme I. It involves initial oxidative insertion of the metal center into one of the primary C–H bonds, yielding **2** via the loose orbiting collision complex **1**. This is followed by a β-hydrogen shift forming **3** and reductive elimination of H_2 via collision complex **4**. The fact that the reactions of ethane with $(OC)_3Mn^-$ and $(OC)_2Fe^-$ had low reaction efficiencies ($\sim$0.01) requires that a barrier separates complex **1** and insertion product ion **2** with reversibility in the oxidative insertion step into the C–H bond.

The multiple H/D exchanges observed in the reaction of $(OC)_3Mn(\pi\text{-}C_2H_4)^-$ with D_2 give insight into the various steps in Scheme I since we enter the same potential energy surface from the product direction. This result not only supports the π-C_2H_4 structure for this product ion in eq 5 but establishes the reversibility of each of the steps between intermediate **2** and the products in Scheme I. However, the equilibrium between **4** and the products is omitted from Scheme I since once separated $(OC)_nM(\pi\text{-}C_2H_4)^-$ will not find an H_2 molecule due to the very low concentrations of these products ($<10^7$ molecules cm^{-3}) in the flow ($>10^{16}$ He atoms cm^{-3}) and short time frame (few milliseconds) of the experiments.

We note that the bimolecular reactions 5 and 7 occurred with similar rate constants and reaction efficiencies. This suggests that similar barriers separate **1** and **2**, and **3** and **4** for M = Mn and $n = 3$. Further, the steps in the equilibria in eq 9 must be com-

$$\underset{\mathbf{3}\text{-}d_2}{[(OC)_3Mn(D)_2(\pi\text{-}C_2H_4)^-]} \rightleftharpoons \underset{\mathbf{2}\text{-}d_2}{[(OC)_3Mn(D)(CH_2CH_2D)^-]} \rightleftharpoons \underset{\mathbf{3}\text{-}d_2'}{[(OC)_3Mn(D)(H)(\pi\text{-}C_2H_3D)^-]} \quad (9)$$

petitive with the ejection of D_2 from **3**-d_2 or HD from **3**-d_2' to allow for such extensive H/D scrambling to be observed. These factors could allow for up to two H/D exchanges per reactive collision. The rearrangement of deuterium from the metal in **3**-d_2 to carbon in **3**-d_2' is statistically and energetically (zero-point energy) favored.[32]

Rather than statistically correcting the measured k_{total} for the six identical primary C–H bonds in C_2H_6 as was done in the condensed-phase oxidative insertion studies,[5,6] we will correct the reaction efficiency (RE). The RE is defined as k_{total}/k_{ADO} where k_{ADO} is the collision-limited rate constant calculated by use of the average dipole orientation theory;[33] k_{ADO} corrects for the polarizability and the dipole moment (e.g., isobutane) of the different alkanes. Since these values will be used to predict rate constants of several higher molecular weight alkanes, the corrected RE per type and number of C–H bonds in the alkane accounts for these variables. The statistically corrected RE for reactions 5 and 6 are RE/(1° C–H bond) = 1.5×10^{-3} and 2.5×10^{-3}, respectively (Table IV).

Table IV. Reaction Efficiencies per C–H Bond Type Derived from the Reactions of $(OC)_3Mn^-$ and $(OC)_2Fe^-$ with Certain Alkanes and Cycloalkanes

		RE/(C–H bond type)	
alkane	type of C–H bond	$(OC)_3Mn^-$	$(OC)_2Fe^-$
C_2H_6	primary	1.5×10^{-3}	2.5×10^{-3}
c-C_5H_{10}	secondary	1.1×10^{-2}	2.1×10^{-2}
c-C_6H_{12}	secondary	3.3×10^{-3}	2.1×10^{-3}
$(CH_3)_3CH$	primary	1.5×10^{-3} [a]	2.5×10^{-3} [a]
	tertiary	2.0×10^{-2} [b]	1.5×10^{-2} [c]

[a] Assumed on the basis of the reactions with C_2H_6. [b] (RE/3° C–H bond))/(RE/(1° C–H bond)) = 13. [c] (RE/(3° C–H bond))/(RE/(1° C–H bond)) = 6.

We note that the k_{total} and RE for these reactions have contributions not only from the oxidative insertion step but also from subsequent steps in these dehydrogenation reactions. Evidence on this point will be discussed in the section involving the reactions with propane-2,2-d_2.

Reactions with Cyclopentane and Cyclohexane. Determination of the related rate constants involving secondary C–H bonds was our next target. The substrates used in these experiments were c-C_5H_{10} and c-C_6H_{12}. Both $(OC)_3Mn^-$ and $(OC)_2Fe^-$ reacted with these neutral hydrocarbons, forming the corresponding (adduct $- H_2)^-$ ion products.

The two ion products $(OC)_3Mn(C_5H_8)^-$ and $(OC)_3Mn(C_6H_{10})^-$ failed to behave as the expected 16-electron cycloalkene complexes in that no reactions were observed with D_2, SiH_4, $(CH_3)_3SiH$, and H_2S as had been observed with $(OC)_3Mn(\pi\text{-}C_2H_4)^-$ formed in reaction 5. Even though the cycloalkene was replaced in the reactions of these (adduct $- H_2)^-$ products with SO_2, a much larger concentration of SO_2 was needed to effect these ligand substitution reactions (smaller relative rate constants) than was required for the reaction of $(OC)_3Mn(\pi\text{-}C_2H_4)^-$ with SO_2. These results lead us to conclude that in the intermediate 16-electron olefin adducts Mn has oxidatively inserted into an allylic C–H bond to yield the corresponding 18-electron hydrido(η^3-allyl)metal complex negative ions shown in eq 10 with c-C_5H_{10}. Related rearrangements will be discussed in later sections of this paper.

$$\underset{m/z\ 139}{(OC)_3Mn^-} + \text{c-}C_5H_{10} \xrightarrow{-H_2} [(OC)_3Mn(\pi\text{-c-}C_5H_8)^-] \rightarrow \underset{m/z\ 207}{(OC)_3Mn(H)(\eta^3\text{-c-}C_5H_7)^-} \quad (10)$$

The analogous ion/molecule reactions with the (adduct $- H_2)^-$ product ions formed in the reactions of $(OC)_2Fe^-$ with the two cycloalkanes were not determined.

The availability of c-C_6D_{12} allowed for the determination of the kinetic deuterium isotope effects for these two dehydrogenation reactions. From the kinetic data in Tables I and II, $k_{c\text{-}C_6H_{12}}/k_{c\text{-}C_6D_{12}} = 3.4 \pm 0.8$ for $(OC)_3Mn^-$, while $k_{c\text{-}C_6H_{12}}/k_{c\text{-}C_6D_{12}} = 5.0 \pm 0.8$ for $(OC)_2Fe^-$. The larger isotope effects observed with cyclohexane compared to those with ethane could indicate more extensive C–H bond cleavage in the oxidative insertion steps with cyclohexane and/or different contributions from subsequent steps to the overall isotope effect.

From the kinetic data in Tables I and II, it is immediately obvious that the rate constant for reaction with the secondary C–H bonds of cyclopentane is greater than that for the C–H bonds of cyclohexane. The statistically corrected RE/(2° C–H bond) values for these two cycloalkanes are listed in Table IV. The significant difference in the reactivities of the secondary C–H bonds in these two cycloalkanes in these overall dehydrogenation reactions is apparent. While RE/(2° C–H bond) values for the c-C_6H_{12} reactions with $(OC)_3Mn^-$ and $(OC)_2Fe^-$ are about the same as the RE/(1° C–H bond), RE/(2° C–H bond) derived

(32) For the IR stretching frequencies of metal hydride bonds, ν_{MH} 2200–1600 cm^{-1} (Collman, J. P.; Hegedus, L. S.; Norton, J. R.; Finke, R. G. *Principles and Applications of Organotransition Metal Chemistry*; University Science Books: Mill Valley, CA, 1987; p 83) and ν_{MH} 2300–1700 cm^{-1} (Kubas, G. J. *Acc. Chem. Res.* **1988**, *21*, 120).

(33) Su, T.; Bowers, M. T. In *Gas Phase Ion Chemistry*; Bowers, M. T., Ed.; Academic Press: New York, 1979; Vol. 1, Chapter 3.

Table V. Measured and Calculated Reaction Efficiencies for the Reactions of $(OC)_3Mn^-$ and $(OC)_2Fe^-$ with the *n*-Alkanes

	$(OC)_3Mn^-$				$(OC)_2Fe^-$			
n-alkane	$RE_{rel}^{cor\,a}$	RE[b]	$RE_{calcd}{}^{I\,c}$	$RE_{calc}{}^{II\,d}$	$RE_{rel}^{cor\,a}$	RE[e]	$RE_{calc}{}^{I\,c}$	$RE_{calc}{}^{II\,e}$
ethane	1.0	9.2×10^{-3}			1.0	1.5×10^{-2}		
propane	2.1	2.5×10^{-2}	3.1×10^{-2}	1.6×10^{-2}	2.0	3.9×10^{-2}	5.7×10^{-2}	1.9×10^{-2}
butane	3.1	4.6×10^{-2}	5.3×10^{-2}	2.2×10^{-2}	5.2	1.3×10^{-1}	9.9×10^{-2}	2.3×10^{-2}
pentane	5.6	1.0×10^{-1}	7.5×10^{-2}	2.9×10^{-2}	5.3	1.6×10^{-1}	1.4×10^{-1}	2.8×10^{-2}
hexane	5.2	1.1×10^{-1}	9.7×10^{-2}	3.6×10^{-2}				
heptane	8.3	2.0×10^{-1}	1.2×10^{-1}	4.2×10^{-2}				

[a] Reaction efficiency (RE) for the reaction divided by the total number of C–H bonds in the alkane relative to the value for ethane (RE/1° C–H bond). [b] RE from Table I. [c] Calculated from RE for C_2H_6 plus [(the number of 2° C–H bonds) (RE/(2° C–H bond)] derived from the reaction with c-C_5H_{10} (Table IV). [d] Calculated as in *b*, but with RE/(2° C–H bond) derived from the reaction with c-C_6H_{12} (Table IV). [e] RE from Table II.

from reactions with c-$C_5H_1{}^0$ are 8 times larger than the corresponding RE/(1° C–H bond).

Similar, but smaller differences were observed in the statistically corrected relative rate constants for oxidative insertion of (η^5-c-$C_5(CH_3)_5$)M($P(CH_3)_3$) (M = Ir or Rh) with these two cycloalkanes in the condensed phase.[2b,5,6] With the same C–H bond dissociation energies in the two cycloalkanes,[34] the authors suggested that the C–H bonds in rings smaller than cyclohexane were more spherically accessible for oxidative insertion.[2b] While this might be true for the small differences observed for these two cycloalkanes in the condensed phase (e.g., k_{rel}(c-C_5H_{10})/k_{rel}(c-C_6H_{12}) = 1.5), additional factors are likely operating in the present results leading to larger effects *if the subsequent step of the β-hydride shift contributes to the rate constant.* One such factor might be the larger relief of strain energy (E_s) in yielding the cyclopentene ligand rather than the cyclohexene ligand; E_s(c-C_5H_{10}) − E_s(c-C_5H_8) = 2.1 kcal mol^{-1} while (E_s(c-C_6H_{12}) − E_s(c-C_6H_{10})) = 0.6 kcal mol^{-1}.[35]

Reactions with Propane. As expected, both $(OC)_3Mn^-$ and $(OC)_2Fe^-$ reacted with propane to yield the corresponding (adduct − H_2)$^-$ product ions at *m/z* 181 and 154, respectively (eqs 11 and 12). The failure of the Mn product ions at *m/z* 181 to react with

$$\underset{m/z\ 139}{(OC)_3Mn^-} + C_3H_8 \rightarrow \underset{m/z\ 181}{(OC)_3Mn(H)(\eta^3\text{-}C_3H_5)^-} + H_2 \quad (11)$$

$$\underset{m/z\ 112}{(OC)_2Fe^-} + C_3H_8 \rightarrow \underset{m/z\ 154}{(OC)_2Fe(H)(\eta^3\text{-}C_3H_5)^-} + H_2 \quad (12)$$

H_2, D_2, SiH_4, $(CH_3)_3SiH$, and H_2S suggests that the structure of this ion is the 18-electron hydrido(η^3-allyl)metal complex negative ion, analogous to the structures proposed for the (adduct − H_2)$^-$ product ions formed from c-C_5H_{10} and c-C_6H_{12}. The adduct ion product at *m/z* 181 from the reaction of $(OC)_3Mn^-$ with propene showed the same reactivity with added neutral substrates as did the product ions of this mass from reaction 11.

The ligand substitution reaction of the *m/z* 181 ions with SO_2[31] (eq 13) formed $(OC)_3Mn(SO_2)^-$. The rate constant for reaction

$$\underset{m/z\ 181}{(OC)_3Mn(H)(\eta^3\text{-}C_3H_5)^-} + SO_2 \rightarrow \underset{m/z\ 203}{(OC)_3Mn(SO_2)^-} + C_3H_6 \quad (13)$$

13 was found to be ~70 times smaller than that measured for the corresponding displacement of C_2H_4 from the 16-electron complex $(OC)_3Mn(\pi\text{-}C_2H_4)^-$ (eq 8; Table III). This considerably smaller rate constant for reaction 13 agrees with our assigned structure of the (adduct − H_2)$^-$ ions at *m/z* 181 being the 18-electron hydrido–η^3-allyl complex and the fact that a barrier exists to the ligand substitution reaction. Since the 18-electron complex $(OC)_5Mn^-$ does not react with SO_2 ($k < 10^{-13}$ cm^3 molecule^{-1} s^{-1}), reaction 13 may be occurring by reversing the insertion of Mn into the allylic C–H bond ([$(OC)_3Mn(H)(\eta^3\text{-}C_3H_5)$] ⇄ [$(OC)_3Mn(\pi$-propene)$^-$]) in the collision between the ion and SO_2.[31] This is believed to be the source of the barrier.

The corresponding ion/molecule reactions with the (adduct − H_2)$^-$ product at *m/z* 154 from reaction 12 were not examined.

Determination of RE for reactions 11 and 12 provides our first test of the utility of the above RE/(C–H bond type) in predicting RE (and rate constants) for the reactions of $(OC)_3Mn^-$ and $(OC)_2Fe^-$ with alkanes. The measured REs for reactions 11 and 12 are smaller than $RE_{calc}{}^{I}$ with use of Re/(2° C–H bond) derived from c-C_5H_{10} (Table V); using RE(2° C–H bond) derived from c-C_6H_{12} underestimated RE for these two reactions by larger differences. As can be seen in the RE_{calc} data in Table V, the RE/(2° C–H bond) determined from the reactions of $(OC)_3Mn^-$ and $(OC)_2Fe^-$ with c-C_6H_{12} yield unreasonably low estimates of RE for the reactions of the two MCMEU metal complex negative ions with the *n*-alkanes listed. While these reactions have yet to be discussed, these data lead us to conclude that the RE/(2° C–H bond) values derived from the reactions with c-C_5H_{10} are most representative of the reactivity of secondary C–H bonds in these reactions.

The reactions of $(OC)_3Mn^-$ and $(OC)_2Fe^-$ with propane-*2,2-d*$_2$ were carried out to see if additional information about the mechanism could be gained from the products and kinetic isotope effects. The results of the reactions with propane-*2,2-d*$_2$ are given in eqs 14 and 15. The products from both reactions showed

$$\underset{m/z\ 139}{(OC)_3Mn^-} + CH_3CD_2CH_3 \xrightarrow{0.47} \underset{m/z\ 182}{(OC)_3Mn(C_3H_5D)^-} + HD \quad (14a)$$

$$\xrightarrow{0.53} \underset{m/z\ 183}{(OC)_3Mn(C_3H_4D_2)^-} + H_2 \quad (14b)$$

$$\underset{m/z\ 112}{(OC)_2Fe^-} + CH_3CD_2CH_3 \xrightarrow{0.73} \underset{m/z\ 155}{(OC)_2Fe(C_3H_5D)^-} + HD \quad (15a)$$

$$\xrightarrow{0.27} \underset{m/z\ 156}{(OC)_2Fe(C_3H_4D_2)^-} + H_2 \quad (15b)$$

significant formation of the (adduct − HD)$^-$ ions at *m/z* 182 and 155 along with extensive generation of the (adduct − H_2)$^-$ ions at *m/z* 183 and 156, respectively.

The ion products at *m/z* 182 (eq 14a) and 155 (eq 15a) must arise by vicinal dehydrogenation; that is, insertion into a C–D or C–H bond followed by a β-shift of hydrogen or deuterium and reductive elimination of HD. However, the product ions at *m/z* 183 (eq 14b) and 156 (eq 15b) could arise either (1) by H/D scrambling in intermediate complexes or (2) by geminal dehydrogenation via a 16-electron carbene complex. The geminal dehydrogenation via metal–carbene complexes appears not to be correct in that (i) there is too much of it in eq 14, (ii) we do not observe any of the (adduct − D_2)$^-$ product ion expected from geminal dehydrogenation at the secondary carbon center, and (iii) metal–carbene formation was not observed in the reaction of $(OC)_2Fe^-$ with neopentane. Further, a carbene–olefin rearrangement would be required to yield the 18-electron product ions determined in reaction 11. Therefore, we conclude that H/D scrambling occurs in the intermediate complexes of these reactions.

The $RE_{calc}{}^{I}$ values (with use of RE/(2° C–H bond) from c-C_5H_{10}) for reactions 11 and 12 involve ~70% of the initial ox-

(34) McMillen, D. F.; Golden, D. M. *Ann. Rev. Phys. Chem.* **1982**, *33*, 493.

(35) Wiberg, K. B. In *Determination of Organic Structures by Physical Methods*; Nachod, F. C., Zuckerman, J. J., Eds.; Academic Press: New York, 1971; Vol. 3, Chapter 4.

Scheme II

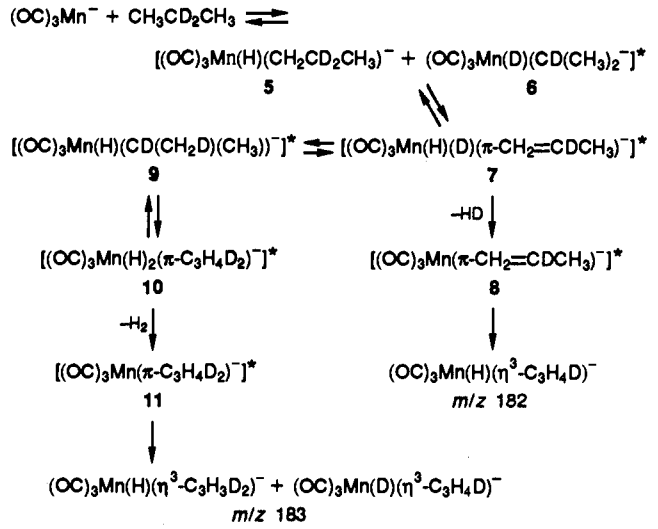

idative insertion occurring at the secondary C–H bonds of propane. If we assume an isotope effect of 3 for the reaction of the secondary C–D bonds of propane-*2,2-d*$_2$ (observed for the reactions of $(OC)_3Mn^-$ with c-C_6H_{12} and c-C_6D_{12}), the net isotope effect for reactions 11 and 14 would be ~2. The observed normal isotope effect for reaction 14 was 1.2 ± 0.2, considerably smaller than expected. The reactions of $(OC)_2Fe^-$ with these two propane molecules proceeded with only slightly increased rate constants and exhibited a similar small isotope effect, 1.0 ± 0.2, within the error limits. Taken together with the H/D scrambling observed in the reaction of $(OC)_3Mn(\pi\text{-}C_2H_4)^-$ with D_2, these results show that the mechanism is more complex than simple rate-limiting insertion of the metal center into the C–H or C–D bonds of the alkane *with two or more steps partially controlling the rate constants and the isotope effects.*

The mechanism to account for these data is presented in Scheme II with use of the results of reaction 14 as the specific example. The loose orbiting collision complexes at the entrance and exit channels have been omitted for brevity. The fact that none of the total adduct structures shown in brackets are observed as ion products means that their lifetimes are $<10^{-8}$ s, which is the time required for the first collision between the ion and a helium atom under these flow conditions. This value is also the lower kinetic limit of the intramolecular rearrangement and H_2 reductive elimination steps involving the intermediates in these reactions.

Since only 2 out of every 100 collisions yield product, the equilibrium in the bimolecular entrance channel of Scheme II producing **5** and **6** is appropriate. A normal isotope effect of unknown magnitude would be expected for this equilibrium since **5** and **6** are formed by oxidative insertion into the primary C–H bonds and the secondary C–D bonds, respectively, of propane-*2,2-d*$_2$.

The equilibrium between **5** and **6** with **7** was established in the H/D exchanges observed in the reaction of the $(OC)_3Mn(\pi\text{-}C_2H_4)^-$ complex with D_2. The rearrangement of **5** to **7** involves migration of a deuterium from C_2 of the *n*-propyl-*2,2-d*$_2$ ligand to the metal. A normal isotope effect is expected for this equilibrium due to the significant difference in the zero-point energies (ΔZPE) in the C–H(D) vs the M–H(D) bonds.[32,36] This will be increased somewhat by the conversion of the remaining C_2–D bond in the *n*-propyl-*2,2-d*$_2$ ligand in **5** from sp^3 to sp^2 hybridization[36] in the olefin ligand in **7**. A similar small normal isotope effect on the **6** to **7** equilibrium would be expected as the alkyl ligand is converted to the π-alkene ligand,

Reductive elimination of HD from **7** would give the 16-electron olefin complex **8**, which inserts Mn into an allylic C–H bond yielding the observed 18-electron hydrido–π-allyl negative ion product at *m/z* 182. This latter step is not involved in the rate of this reaction.

The H/D scrambling is believed to occur via **7** competitive with HD loss. If **D** migrates from Mn in **7** to the terminal CH_2 of the olefin, complex **9** will result. This migration is favored by the ΔZPE[32,36] (Mn–D bond in **7**, but C–D bond in **9**) and by formation of the stronger primary C–D bond in **9** compared to the weaker secondary C–D bond in **5** if D were to migrate to C_2 of the olefin.[37] A β-hydride shift in **9** yields **10**, which can extrude H_2 and ultimately produce the ion product at *m/z* 183, retaining both deuterium atoms.

The equilibrium rearrangement of **7** to **10** will be favored by the ΔZPE in converting M–D and C–H bonds in **7** to M–H and C–D bonds in **10**. If we assume similar stretching frequencies in these metal complex negative ions and neutral complexes,[32] this equilibrium favors **10** by 0.5 kcal mol^{-1} based solely on the stretches assuming ν_{MH} 2000 cm^{-1}. This analysis leads to the conclusion that D prefers being bound to C rather than to the metal. The additional outlet channel available with the propane-*2,2-d*$_2$ molecule involving preequilibrium formation of intermediate **10**, which possesses increased zero-point energy relative to the precursor **7**, can lead to an *inverse isotope effect* for this outlet channel.[38] The magnitude of this inverse isotope effect will depend on the ΔZPE and is a function of ν_{MH} (M = Mn or Fe), which are unknown for these intermediate negative ions. *However, to use this inverse isotope effect of the outlet channel forming **11** via **10** to reduce the normal isotope effect expected for forming **8** via **7** requires that the barriers for the reductive elimination of H_2 and HD partially contribute to the rate constant.*

That the barriers for the unimolecular β-hydrogen and β-deuterium shifts and their retro processes are significant is seen in the following argument. Statistically, the ratio [*m/z* 183 (loss of H_2)]/[*m/z* 182 (loss of HD)] from propane-*2,2-d*$_2$ should be 3/2, which is close to the observed ratio of 53/47 in reaction 14. However, this statistical ratio does not take into account the energetic preference for **10** vs **7** discussed previously, which suggests that equilibration of the intermediates **7** and **10** is not complete.

The above mechanism and energetic considerations also explain the final question of why the (adduct – D_2)$^-$ product ions were not observed in reactions 14 and 15. This would require the equilibria shown in eq 16. The retro β-shift of H on Mn in **7**

$$\mathbf{7} \rightleftarrows \underset{\mathbf{12}}{(OC)_3Mn(D)(CH_2CHDCH_3)^-} \rightleftarrows \underset{\mathbf{13}}{(OC)_3Mn(D)_2(\pi\text{-}CH_2{=}CHCH_3)^-} \quad (16)$$

to C_2 of the propene-*2-d*$_1$ ligand yielding **12** is *less* favorable than the **7** ⇄ **6** equilibrium (weaker secondary vs stronger primary C–H bond formation)[37] and the **7** ⇄ **9** equilibrium because of this same factor plus the ΔZPE.[32,36] This means that the formation of **12** (and, therefore, **13**) effectively does not occur.

The results of the reaction of $(OC)_2Fe^-$ with propane-*2,2-d*$_2$ (eq 15) were similar to those with $(OC)_3Mn^-$. The overall kinetic isotope effect, $k_{C_3H_8}/k_{(CH_3)_2CD_2}$ = 1.0 ± 0.2, is the same value within the error limits as that determined for reaction 14 (Table II). The significant amount of the (adduct – H_2)$^-$ product forming channel (eq 15b) was smaller than that found in reaction 14b. We note that none of the (adduct – D_2)$^-$ product ion was observed. A similar mechanism to that described in Scheme II is suggested for the formation of the two product ions in reaction 15. However, equilibration of the intermediates in the (adduct – HD)$^-$ and the (adduct – H_2)$^-$ product forming channels in reaction 15 is less complete than was observed in reaction 14.

The larger isotope effects observed in the reactions of $(OC)_2Fe^-$ vs $(OC)_3Mn^-$ with ethane and cyclohexane suggest that $\nu_{FeH} < \nu_{MnH}$ in the intermediates leading to the $(OC)_nM(\pi\text{-}C_3H_6)^-$ ions.[39]

(36) Bellamy, L. J. *The Infrared Spectra of Complex Molecules*, 2nd ed.; Wiley: New York, 1960.

(37) $D°(n\text{-}C_3H_7\text{–H})$ = 98 kcal mol^{-1}, $D°(i\text{-}C_3H_7\text{–H})$ = 94.5 kcal mol^{-1}, and $D°(t\text{-}C_4H_9\text{–H})$ = 92 kcal mol^{-1} are listed in: Benson, S. W. *Thermochemical Kinetics*, 2nd ed.; Wiley: New York, 1976; p 309.

(38) See ref 6 and references therein.

Such a difference could have a major influence on the $(OC)_2Fe(H)(D)(\pi\text{-}C_3H_5D)^- \rightleftarrows (OC)_2Fe(H)_2(\pi\text{-}C_3H_4D_2)^-$ rearrangement, producing a larger ΔZPE and an increased contribution of the inverse isotope effect than that in reaction 14. The reduced extent of the equilibration in reaction 15 vs reaction 14 would be offset by the greater contribution of the inverse isotope effect in reaction 15. Thus, a balancing of normal and inverse isotope effects on the two product-forming channels in these two reactions is suggested.

Reactions with Higher Molecular Weight *n*-Alkanes. Periana and Bergman[6] reported that they found a direct correlation between the relative rate constants for the oxidative insertion reactions of $(\eta^5\text{-c-}C_5(CH_3)_5)Rh(P(CH_3)_3)$ with alkanes and the number of secondary C–H bonds in the alkane. In the present study, the additional reactions of the C_4–C_7 *n*-alkanes with $(OC)_3Mn^-$ and of *n*-butane and *n*-pentane with $(OC)_2Fe^{\bullet-}$ were examined. The $(adduct - H_2)^-$ product ions from the reactions with $(OC)_3Mn^-$ were characterized as the corresponding hydrido$(\eta^3\text{-}C_3H_3R_2)$metal complex negative ions by the data in Table III. The generalized form of the reactions of $(OC)_3Mn^-$ and $(OC)_2Fe^-$ with the *n*-alkanes is given in eq 17.

$$(OC)_xM^- + C_nH_{2n+2} \rightarrow (OC)_xM(H)(\eta^3\text{-}C_nH_{2n-1})^- + H_2 \quad (17)$$

The reaction efficiency data for these reactions in Tables I and II are summarized in Table V. RE_{rel}^{cor} is the relative reaction efficiency (to that of ethane) corrected for the total number of C–H bonds in the alkane and represents the average RE_{rel}/(C–H bond) for the mix of primary and secondary C–H bonds in the individual alkane,[5,6] The general increase in RE_{rel}^{cor} is consistent with the greater reactivity of the secondary C–H bonds in these reactions, *This result eliminates RE/(2° C–H bond) derived from the reactions of the two MCMEU metal complex negative ions with c-C_6H_{12} as representative of secondary C–H bonds in these reactions*, We observe roughly a doubling of RE_{rel}^{cor} between ethane and *n*-pentane in the more extensive data set with $(OC)_3Mn^-$, However, this large increase in RE_{rel}^{cor} vanished for the reaction with *n*-hexane but was again observed for the reaction with *n*-heptane. At first glance, this break in RE_{rel}^{cor} appeared to be a problem with the rate constant for the *n*-hexane reaction. However, when we compare the measured RE with RE_{calc}^{1}, we find that the reaction of $(OC)_3Mn^-$ with *n*-pentane is too fast while that for *n*-hexane is close to that predicted. The RE for the reaction of $(OC)_3Mn^-$ with *n*-heptane again shows an increase over the RE_{calc}^{1}. In the more limited study of the reactions of $(OC)_2Fe^-$ with the *n*-alkanes, the largest error between RE and RE_{calc}^{1} occurred in the propane reaction with good agreement in the reactions of butane and pentane.

The reactions of $(OC)_3Mn^-$ with *n*-heptane and $(OC)_2Fe^-$ with propane have the largest differences between RE and RE_{calc}^{1} in Table V, While outside of our experimental errors, these differences are only 45 and 54%, respectively, of RE for these two reactions, Therefore, the additivity of the separate RE/(C–H bond type) for the contributions of the number of primary and secondary C–H bonds works quite well in predicting the overall reaction efficiencies for these *n*-alkane molecules.

The approximate correlation of the gas-phase data compared to the linear correlation reported for the condensed-phase C–H bond oxidative insertions with these alkanes is consistent with our analysis that the present data involve contributions from the further steps producing dehydrogenation to the RE. We believe that the magnitude of the RE is largely controlled by the initial oxidative insertion step. While the kinetic contributions of subsequent steps will be similar to those steps present in the models for the primary (C_2H_6) and secondary C–H bonds (c-C_5H_{10}), small perturbations should be expected to alter these barrier heights as the alkane is varied, leading to correlation deviations. For example, *trans*-alkene ligand formation is likely with the C_4–C_7 *n*-alkanes, which is not possible in the c-C_5H_{10} model for RE/(2° C–H bond) leading to a lower barrier for the β-hydride shift. Further, a small increase in the β-hydride shift barrier may result for a stronger primary vs a weaker secondary C–H bond in the intermediate $(OC)_xM$–C–C–H$^-$ species. This latter point might explain why $RE < RE_{calc}^{1}$ for the two reactions with propane.

Reactions with Isobutane. The isobutane molecule is interesting because it has nine identical primary C–H bonds and a single tertiary C–H bond. The results obtained with the homologous series of *n*-alkanes supported the RE/(1° C–H bond) values determined from the reactions of $(OC)_3Mn^-$ and $(OC)_2Fe^-$ with ethane. Therefore, we should be able to evaluate the reactivity of the tertiary C–H bond in isobutane on the basis of these values.

As expected, the reactions of $(OC)_3Mn^-$ and $(OC)_2Fe^-$ with isobutane formed the corresponding $(adduct - H_2)^-$ ions at *m/z* 195 (eq 18) and 168 (eq 19), respectively. The masses of these

$$\underset{m/z\ 139}{(OC)_3Mn^-} + (CH_3)_3CH \rightarrow \underset{m/z\ 195}{(OC)_3Mn(H)(C_4H_7)^-} + H_2 \quad (18)$$

$$\underset{m/z\ 112}{(OC)_2Fe^-} + (CH_3)_3CH \rightarrow \underset{m/z\ 168}{(OC)_2Fe(C_4H_7)^-} + H_2 \quad (19)$$

two product ions were the same as those of $(OC)_5Mn^-$ and $(OC)_4Fe^-$ ions, respectively, which were also present in the separate flows. This fact does not present a problem for observing the product from reactions 18 and 19. Since $(OC)_{4,5}Mn^-$ and $(OC)_{3,4}Fe^-$ do not react with the hydrocarbon, the increases in the ion signal intensity at *m/z* 195 and 168, respectively, are due to product formation. However, a problem exists in trying to determine the further ion/molecule chemistry of the $(adduct - H_2)^-$ product in reaction 19 with SO_2 since $(OC)_{3,4}Fe^-$ reacts rapidly with SO_2 to form a complex mixture of product ions.

This is not a problem in reaction 18 because the amount of $(OC)_5Mn^-$ present in the flow is small (see Figure 1) and it does not react with SO_2. Thus, the structure elucidation for the product ions from reactions 18 and 19 was done with the Mn derivative at *m/z* 195. The absence of reaction of the $(adduct - H_2)^-$ at *m/z* 195 formed in reaction 15 with D_2 and H_2S and the smaller rate constant for the alkene ligand substitution by SO_2 strongly suggested that these product ions have the 18-electron structure $(OC)_3Mn(H)(\eta^3\text{-2-methylallyl})^-$. This structure is related to the structures of the $(adduct - H_2)^-$ ion products formed in the reactions of $(OC)_3Mn^-$ (and likely also in the reactions of $(OC)_2Fe^-$) with propane, the *n*-alkanes, and the cycloalkanes.

The RE_{calc} for the nine primary C–H bonds in isobutane is 1.3×10^{-2} with $(OC)_3Mn^-$ and 2.2×10^{-2} with $(OC)_2Fe^-$. Subtracting these RE_{calc} values from the RE determined for the two reactions with isobutane yields RE/(3° C–H bond) = 2.0×10^{-2} ($\mathbf{13} \times$ (RE/(1° C–H bond))) for the reaction with $(OC)_3Mn^-$ and 1.5×10^{-2} ($\mathbf{6} \times$ (RE/1° C–H bond))) for the reaction with $(OC)_2Fe^-$ (Table IV).

To support the results of the above kinetic analysis of the greater reactivity of the tertiary vs the primary C–H bonds in the initial oxidative insertion step, the reaction of $(OC)_3Mn^-$ with $(CD_3)_3CH$ was investigated. The products and their branching fractions are given in eq 20. Extensive H/D scrambling in the reaction in-

$$\underset{m/z\ 139}{(OC)_3Mn^-} + (CD_3)_3CH \xrightarrow{0.54} \underset{m/z\ 203}{(OC)_3Mn(D)(\eta^3\text{-}C_4D_7)^-} + HD \quad (20a)$$

$$\xrightarrow{0.46} \underset{m/z\ 202}{(OC)_3Mn(D)(\eta^3\text{-}C_4HD_6)^-} + D_2 + \underset{m/z\ 202}{(OC)_3Mn(H)(\eta^3\text{-}C_4D_7)^-} + D_2 \quad (20b)$$

termediates forming the product ions at *m/z* 202 was observed, which was similar to the results obtained in the reaction of $(OC)_3Mn^-$ with propane-*2,2-d*$_2$. The analogous mechanism to account for these results is shown in Scheme III. As in Scheme II, the loose, orbiting collision complexes in the inlet and outlet channels are omitted for brevity.

(39) Chang, et al. (Chang, S.-C.; Hauge, R. H.; Hafafi, Z. H.; Margrave, J. L.; Billups, W. E. *J. Am. Chem. Soc.* **1988**, *110*, 7975) reported the Fe–H stretch at 1681.6 cm^{-1} and the Fe–D stretch at 1209.2 cm^{-1} in HFeCH and DFeCD, respectively.

Scheme III

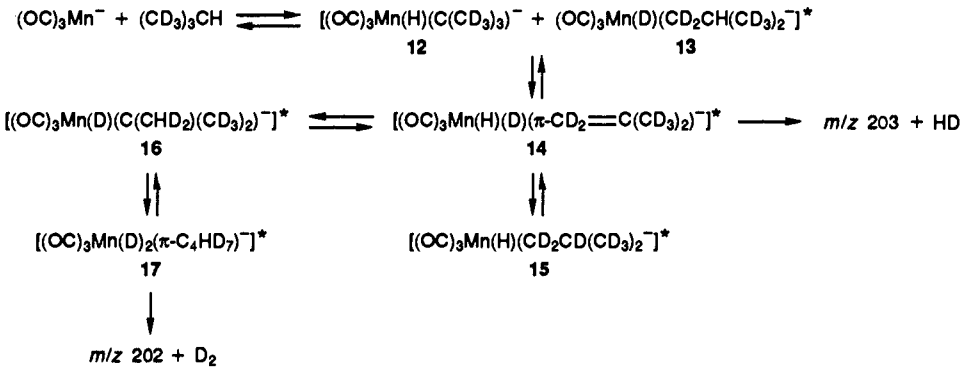

Normal isotope effects are expected for generation of intermediate **13** and the equilibrium formation of **14** from **12**. The retro β-deuteride shift in **14**, which is favored over the retro β-hydride shift by ΔZPE,[32,36] would strongly favor formation of **12** (primary C–D bond formed) rather than **15** (tertiary C–D bond formed) due to the resulting bond dissociation energies.[37] As is seen in Scheme III, **12** and **15** have no choice but to regenerate **14** on their way to yield the products. Reductive elimination of HD from **14** would yield the major product ions at m/z 203 in eq 20a.

The retro β-hydride shift in **14** will strongly favor formation of **16** over **13** because of the resulting C–H bond strengths. While the return of **16** to **14** is favored by the ΔZPE, it is driven forward to produce **17** by the large statistical C_β–D/C_β–H ratio of 8 present in **16**. The equilibrium conversion of **14** $\rightleftarrows$ **17** will exhibit a *normal isotope effect* due to the ΔZPE and is the major difference between Schemes II and III.

From the rate constants for reactions 18 and 20 (Table I), $k_{(CH_3)_3CH}/k_{(CD_3)_3CH} = 1.3 \pm 0.2$ was determined. This small isotope effect is in keeping with the kinetic analysis given above that *the principle oxidative insertion step in reactions 18 and 20 occurred at the single tertiary C–H bond rather than at one of the nine primary C–H bonds.*

The corresponding reaction of $(OC)_2Fe^-$ with $(CD_3)_3CH$ was not examined.

Summary and Conclusions

Only $(OC)_2Fe^-$ was observed to react with methane and neopentane, forming exclusively the corresponding adduct negative ions. The neopentane adduct was characterized as the oxidative insertion product $(OC)_2Fe(H)(CH_2C(CH_3)_3)^-$ on the basis of the results of its further ion/molecule reactions. It is assumed that the more slowly formed adduct negative ion product from the reaction of $(OC)_2Fe^-$ with methane has the related structure $(OC)_2Fe(H)(CH_3)^-$.

Both $(OC)_3Mn^-$ and $(OC)_2Fe^-$ reacted with the other alkanes (n-C_nH_{2n+2} where n = 2–7, $(CH_3)_3CH$, c-C_5H_{10}, and c-C_6H_{12}) studied, All of these hydrocarbons contained C_β–H bonds relative to the potential site(s) for oxidative insertion, and the observed negative ion products were those of dehydrogenation. The (adduct – H_2)$^-$ product ions derived from the reactions of $(OC)_3Mn^-$ with the hydrocarbons were characterized on the basis of the results from their further ion/molecule reactions with D_2 (H/D exchange), SiH_4, $(CH_3)_3SiH$, H_2S (adduct formation), and SO_2 (alkene ligand substitution). Only the (adduct – H_2)$^-$ product ions from the reaction of $(OC)_3Mn^-$ with ethane reacted with the above neutral reactants. These results lead to the conclusion that the structure of these (adduct – H_2)$^-$ ions is the 16-electron ethylene complex $(OC)_3Mn(\pi\text{-}C_2H_4)^-$. Up to four H/D exchanges were observed in the reaction of this (adduct – H_2)$^-$ with D_2, which established the reversibility of the β-hydride shifts occurring in the reaction intermediates.

The other (adduct – H_2)$^-$ product ions formed in the reactions of $(OC)_3Mn^-$ with the remaining eight hydrocarbons failed to react with the above first four neutral reactants and reacted with SO_2 by alkene substitution much slower than did $(OC)_3Mn(\pi\text{-}C_2H_4)^-$. From these results, these eight product ions are assigned the structures of the 18-electron complexes $(OC)_3Mn(H)(\eta^3\text{-}C_3H_3R_2)^-$ where the nature of the R groups in the η^3-allyl ligand varies with the structure of the hydrocarbon molecule used. Formation of these product ions is rationalized by the further oxidative insertion of Mn into an allylic C–H bond in the intermediate 16-electron olefin complexes $(OC)_3Mn(\pi\text{-olefin})^-$.

From the reactions of $(OC)_3Mn^-$ and $(OC)_2Fe^-$ with ethane and cyclopentane, the statistically corrected reaction efficiencies for the reactions involving primary (RE/(1° C–H bond)) and secondary C–H bonds (RE/(2° C–H bond)) are derived (Table IV). From these values, the (RE/(2° C–H bond))(RE/(1° C–H bond)) ratios of 7 ($(OC)_3Mn^-$) and 8 ($(OC)_2Fe^-$) are obtained. These separate contributions to the reaction efficiency per number and type of C–H bonds present in a hydrocarbon have been applied to the reactions of $(OC)_3Mn^-$ and $(OC)_2Fe^-$ with the homologous series n-C_nH_{2n+2} where n = 3–7 (for $(OC)_3Mn^-$) and n = 3–5 (for $(OC)_2Fe^-$). While the resulting RE_{calc} agrees quite well with the measured RE for these reactions, several reasons are suggested to account for deviations in the correlation.

The results of the reactions of $(OC)_3Mn^-$ and $(OC)_2Fe^-$ with propane-2,2-d_2 demonstrated the kinetic complexity of these oxidative insertion–dehydrogenation reactions. On the basis of RE_{calc} for the reactions with C_3H_8, $\sim$ 70% of RE would have occurred by oxidative insertion into the secondary C–H bonds if this step solely controlled the rate. Thus, a significant kinetic deuterium isotope effect would be predicted for the reaction with $(CH_3)_2CD_2$. However, the reactions with both MCMEU metal complex ions exhibited very small isotope effects, and the products, (adduct – HD)$^-$ and (adduct – H_2)$^-$, showed that extensive H/D scrambling had occurred in the reaction intermediates. The formation of significant amounts of the (adduct – H_2)$^-$ product ions suggested that an equilibrium existed between the initially formed complex $(OC)_nM(H)(D)(\pi\text{-olefin-}d_1)^-$ and the $(OC)_nM(H)_2(\pi\text{-olefin-}d_2)^-$ complex. The ΔZPE in these two complexes favors formation of the latter metal–dihydride complex and leads to an *inverse kinetic isotope effect* for the (adduct – H_2)$^-$ product-forming branch. However, to use the inverse isotope effect to essentially negate the normal isotope effect for equilibrium formation of metal–(H)(D) complex ions requires that each of these processes contribute to k_{total} and RE for this reaction. For this to occur, the barriers of the C–H bond oxidative insertion inlet channel and several of these intermediate steps as well as the outlet channel must be of similar magnitudes on the potential energy surface for this dehydrogenation reaction.

Isobutane ($(CH_3)_3CH$) was selected as the model compound to determine the reactivity of a tertiary C–H bond, RE/(3° C–H bond). The reactions of the two metal complex negative ions with isobutane were examined and the (adduct – H_2)$^-$ ion products were characterized as the $(OC)_nM(H)(\pi\text{-}\eta^3\text{-}2\text{-}CH_3\text{allyl})^-$ complexes, Analysis of the RE for these reactions indicated that initial oxidative insertion into a primary C–H bond accounted for only 39% of the reaction with $(OC)_3Mn^-$ and 59% of the reaction with $(OC)_2Fe^-$. The data yield (k/(3° C–H bond))/(k/(1° C–H bond)) ratios of 13 for $(OC)_3Mn^-$ and 6 for $(OC)_2Fe^-$. The small normal isotope effect observed in the reaction of $(OC)_3Mn^-$ with

$(CD_3)_3CH$ supported the greater reactivity of the tertiary vs primary C-H bonds in isobutane toward initial oxidative insertion by the metal center.

The above results lead us to conclude that the relative reactivities of C-H bonds of alkanes in oxidative insertion reactions with $(OC)_3Mn^-$ and $(OC)_2Fe^-$ is *tertiary* ≥ *secondary* > *primary*. This extends the C-H bond relative reactivity scale reported in the condensed phase to include tertiary C-H bonds.[5,6] The apparent absence of oxidative insertion into tertiary C-H bonds in the condensed-phase studies was attributed to steric effects with the $(\eta^5\text{-}C_5Me_5)ML_2$ complexes.[5] While we cannot discount steric effects in the present gas-phase negative ions, the steric effects in reactions with $(OC)_3Mn^-$ and $(OC)_2Fe^-$ should be considerably smaller than those experienced with the condensed-phase complexes containing the bulky $\eta^5\text{-}C_5(CH_3)_5$ ligand. However, such considerations must await structural information for the two MCMEU transition-metal complex negative ions.[40,41]

Acknowledgment. We gratefully acknowledge support for this research from the National Science Foundation and discussions of the isotope effects with Professors D. W. Setser and R. L. Schowen.

(40) Poliakoff and Turner (Poliakoff, M.; Turner, *J. Chem. Soc., Dalton Trans.* **1973**, 1351; **1974**, 2276. Poliakoff, M. *Ibid.* **1974**, 210) determined the structure of $Fe(CO)_3$, which is isoelectronic with $(OC)_3Mn^-$, in low-temperature matrices to be of C_{3v} symmetry with the OC-Fe-CO angle ~110°, slightly distorted from a planar structure.

(41) Guenzburger et al. (Guenzgurger, D.; Saitovitch, E. M. B.; De Paoli, M. A.; Manela, H. *J. Chem. Phys.* **1984**, *80*, 735) reported molecular orbital studies on $Fe(CO)_5$ and its photofragments $Fe(CO)_n$ where n = 1-4. The linear and a bent geometry for $Fe(CO)_2$ were examined.

Global Control of Suprathreshold Reactivity by Quantized Transition States

David C. Chatfield,[†] Ronald S. Friedman,[†] Donald G. Truhlar,*[,†] Bruce C. Garrett,[‡] and David W. Schwenke[§]

Contribution from the Department of Chemistry and Supercomputer Institute, University of Minnesota, Minneapolis, Minnesota 55455-0431, the Molecular Science Research Center, Pacific Northwest Laboratory, Richland, Washington 99352, and the NASA Ames Research Center, Moffett Field, California 94035. *Received April 20, 1990. Revised Manuscript Received August 14, 1990*

Abstract: We present evidence that the accurate quantum mechanical probability of the reaction of H with H_2 is globally controlled by quantized transition states up to very high energies. The quantized transition states produce steplike features in the cumulative reaction probability curves that are analyzed up to energies of 1.6 eV; the analysis clearly associates these steps (or "thresholds") with quantized dynamical bottlenecks that control the passage of reactive flux to products. We have assigned bend and stretch quantum numbers to the modes orthogonal to the reaction coordinate for all these transition states on the basis of threshold energies of semiclassical vibrationally adiabatic potential energy curves and vibrationally specific cumulative reaction probability densities.

1. Introduction

A subject that has received increasing attention over the past several years is the role of transition states[1,2] and phase space structures[3] as dynamical bottlenecks to flux flow in classical mechanics. Some progress is also being made in understanding the relevance of these results to quantum dynamics,[4] and variational and other generalized transition-state theory calculations based on quantized transition states[2,5-7] have proved very successful in reproducing accurate quantum dynamical rate constants. As a result we have gained considerable confidence in the dominance of threshold behavior of chemical reactivity by vibrationally adiabatic dynamical bottlenecks,[5,6,8] and these have been shown to exert control not only at un-state-selected reaction thresholds but also at thresholds for some vibrationally excited reactions.[5a,5h,9] In the present paper we present numerical evidence that quantized dynamical bottlenecks limit the accurate quantum dynamical flux from reactants to products in a chemical reaction in a much more global way.

We have studied the energy dependence of the cumulative reaction probability[10] (hereafter referred to as the CRP) for the H + H_2 reaction for various values of the total angular momentum J. The quantum mechanical CRP, which we denote $N^J_{\alpha\alpha'}(E)$, is defined as the sum over all state-to-state ($n \rightarrow n'$) reactive transition probabilities $P^J_{\alpha n\alpha' n'}(E)$ from a given initial chemical arrangement α to a final chemical arrangement α'

$$N^J_{\alpha\alpha'}(E) = \sum_n \sum_{n'} P^J_{\alpha n\alpha' n'}(E) \quad (1)$$

where n denotes the collection of all initial quantum numbers and n' denotes the set of final ones. For example, for an atom-diatom

[†] University of Minnesota.
[‡] Pacific Northwest Laboratory.
[§] NASA Ames Research Center.

(1) (a) Keck, J. C. *Adv. Chem. Phys.* **1967**, *13*, 85. (b) Pechukas, P.; McLafferty, F. J. *J. Chem. Phys.* **1973**, *58*, 1622. (c) Pollak, E.; Pechukas, P. *J. Chem. Phys.* **1978**, *69*, 1218. (d) Garrett, B. C.; Truhlar, D. G. *J. Phys. Chem.* **1979**, *83*, 1052. (e) Garrett, B. C.; Truhlar, D. G. *J. Phys. Chem.* **1980**, *84*, 805. (f) Chesnavich, W. J.; Su, T.; Bowers, M. In *Kinetics of Ion Molecule Reactions*; Ausloos, P., Ed.; Plenum: New York, 1979; p 31. (g) Chesnavich, W. J.; Bass, L.; Su, T.; Bowers, M. J. *J. Chem. Phys.* **1981**, *74*, 2228. (h) Doll, J. D. *J. Chem. Phys.* **1981**, *74*, 1074.

(2) For a review see: Truhlar, D. G.; Hase, W. L.; Hynes, J. T. *J. Phys. Chem.* **1983**, *87*, 2664, 5523E.

(3) (a) Davis, M. J. *J. Chem. Phys.* **1987**, *86*, 3978. (b) Skodje, R. T.; Davis, M. J. *J. Chem. Phys.* **1988**, *88*, 2429. (c) DeLeon, N.; Mehta, M. A.; Topper, R. Q. Unpublished results.

(4) See, for example: Marcus, R. A. *Ber. Bunsenges. Phys. Chem.* **1977**, *81*, 190. Marston, C. C.; Wyatt, R. E. *ACS Symp. Ser.* **1984**, *No. 263*, 441. Brown, R. C.; Wyatt, R. E. *Phys. Rev. Lett.* **1986**, *57*, 1. Skodje, R. T.; Rohrs, H. W.; VanBuskirk, J. *Phys. Rev. A* **1989**, *40*, 2894, and references cited therein. See also: Gomez Llorente, J. M.; Hahn, O.; Taylor, H. S. *J. Chem. Phys.* **1990**, *92*, 2762.

(5) (a) Garrett, B. C.; Truhlar, D. G. *J. Phys. Chem.* **1979**, *83*, 1079. (b) Truhlar, D. G.; Garrett, B. C. *Acc. Chem. Res.* **1980**, *13*, 440. (c) Truhlar, D. G.; Isaacson, A. D.; Skodje, R. T.; Garrett, B. C. *J. Phys. Chem.* **1982**, *86*, 2252. (d) Rai, S. N.; Truhlar, D. G. *J. Chem. Phys.* **1983**, *79*, 6046. (e) Truhlar, D. G.; Garrett, B. C. *Annu. Rev. Phys. Chem.* **1984**, *35*, 159. (f) Isaacson, A. D.; Sund, M. T.; Rai, S. N.; Truhlar, D. G. *J. Chem. Phys.* **1985**, *82*, 1338. (g) Garrett, B. C.; Truhlar, D. G.; Schatz, G. C. *J. Am. Chem. Soc.* **1986**, *108*, 2876. (h) Garrett, B. C.; Truhlar, D. G.; Varandas, A. J. C.; Blais, N. C. *Int. J. Chem. Kinet.* **1986**, *18*, 1065. (i) Truhlar, D. G.; Garrett, B. C. *J. Chim. Phys.* **1987**, *84*, 365.

0002-7863/91/1513-486$02.50/0